Fiducial Reference Measurements for Ground-Based DOAS Air-Quality Observations

ESA Contract No. 4000135355/21/I-DT-lr

<u>Deliverable D8.2</u>

ATBD
BrO stratospheric profiling

Date: Friday 5th June, 2026
Version: 2.0

Stratospheric BrO profiling ATBD v2

Martina M. Friedrich, Michel Van Roozendael, Thomas Wagner, Alkis Bais, Steffen Beirle, Caroline Fayt, Udo Frieß, Dimitris Karagkiozidis, Kai Krause, Alexis Merlaud, Mónica Navarro-Comas, Gaia Pinardi, Ankie Piters,Cristina Prados-Roman, Olga Puentedura, Andreas Richter, Margarita Yela

Friday 5th June, 2026

Acronyms

4D-Var four-dimensional variational chemical assimilation.

AK Averaging kernel.

AMF air mass factor.

BASCOE Belgian Assimilation System for Chemical ObsErvations.

CTM Chemical transport Model.

DISORT DIScrete Ordinate Radiative Transfer.

DOAS Differential Optical Absorption Spectroscopy.

DOF Degrees of Freedom.

DSCD Differential Slant Column Density.

ECMWF European Centre for Medium-Range Weather Forecasts.

EnKF ensemble Kalman filter.

FRM4DOAS Fiducial Reference Measurements for Ground-Based DOAS Air-Quality Observations.

FWHM Full Width at Half Maximum.

GEOMS Generic Earth Observation Metadata Standard.

los line of sight.

LUT Look-up table.

MAX-DOAS Multi-Axis DOAS.

MIPAS Michelson Interferometer for Passive Atmospheric Sounding.

MYSTIC Monte Carlo code for the physically correct tracing of photons in cloudy atmosphere.

NDACC Network for the Detection of Atmospheric Composition Changes.

OEM Optimal Estimation Method.

PSC polar stratospheric cloud.

RMS Root mean square.

RTM Raditative Transfer Model.

SCD slant column density.

SLIMCAT Single Layer Isentropic Model of Chemistry and Transport.

SZA Solar zenith angle.

toa top of atmosphere.

UTC Coordinated Universal Time.

UV ultraviolet.

VCD Vertical Column Density.

WP Work package.

Contents

1 Introduction

This document constitutes and update to Deliverable:D8.2v.1. This document is a self-contained document, describing the aspects presented in the previous version and extending it to include new aspects. Smaller changes have been made in Sect. 1 (this section) and Sect. 2. Extensive additions were made to Sect. 6.

We describe the algorithm used to retrieved stratospheric columns and vertical profiles of BrO, based on zenith-sky radiance measurements recorded around twilight in the UV spectral range. This algorithm is similar in concept to the stratospheric NO_2 profile algorithm already implemented in the Fiducial Reference Measurements for Ground-Based DOAS Air-Quality Observations (FRM4DOAS) system, however it also differs in several important respects that are further detailed in the document.

Retrievals exploiting zenith measurements at high Solar zenith angle (SZA) are different from Multi-Axis DOAS (MAX-DOAS) measurements for tropospheric retrieval in several ways:

- The change in the light path between different measurements is not induced by a change of viewing direction but instead by changes of the suns position:
  - The last scattering (of light that reaches the instrument) takes place at a position directly above the instrument
  - The effective height of the last scattering determines at which height the box air mass factor (AMF) is the largest.
- Different altitudes receive different solar energy hence introducing complex differences in the photo-chemistry at different times $\longrightarrow$ The concentration at each altitude is a function of local SZA, the profile needs to be considered along the line of sight (los)

At high SZA ($80^\circ - 92^\circ$), the multiple-scattering light paths[1] through the stratosphere become long and altitude-selective, strongly enhancing sensitivity to BrO absorption between roughly 15 and 30 km (Solomon et al., 1987). This geometry-driven gain in stratospheric sensitivity has been characterized in numerous twilight Differential Optical Absorption Spectroscopy (DOAS) studies (e.g. Bassford et al., 2005; Aliwell et al., 2002). Given the fast and complex photo-chemical processes influencing the concentration of BrO when light conditions change, a retrieval algorithm for BrO has to include a step of modelling the photo-chemical processes (e.g. Hendrick et al., 2007), additionally to the modelling of the light traversing the atmosphere. The conceptual outline of a BrO stratospheric retrieval is hence:

1. Record noon and twilight light spectra in the ultraviolet (UV) range.
2. Perform DOAS fit analysis to get measured Differential Slant Column Density (DSCD).
3. Produce *a priori* profiles of BrO as a function of SZA by means of a Chemical transport Model (CTM) at the measurement SZAs.
4. Use a radiative transfer model capable of using these *a priori* at different SZAs to consider correct profiles along the los and calculate slant column density (SCD) as well as weighting functions.
5. Use the measured DSCD, the *a priori* profiles of BrO, the simulated SCDs at the SZAs of the measurements and the time of reference, together with the weighting functions in a 1-step inversion to retrieve the profile at a determined SZA.

In Sect. 2 we describe the overall retrieval strategy. Details on the DOAS fit (step 2 above), such as recommended retrieval windows and absorption cross-sections can be found in FRM4DOAS-2.0:D8.1. In Sect. 3 we briefly describe our choice of CTM, Belgian Assimilation System for Chemical ObsErvations (BASCOE). In Sect. 4 we outline the forward model used (DIScrete Ordinate Radiative Transfer (DISORT) Stamnes et al., 1988) as well as the wrapper package `uvspec` that handles the SZA dependent profiles and accordingly, the integration along the los, the Jacobian calculation and the constructions of the direct DISORT input layer properties. In Sect. 5 we contrast the current approach with approaches previously applied in the literature as well as with the stratospheric NO_2 retrieval currently implemented in FRM4DOAS. In Sect. 6 we test our algorithm, mostly for Harestua, but also to a limited extend at Lauder and Kiruna, and compare it in the case of Harestua to previously retrieved stratospheric profiles and and Vertical Column Densitys (VCDs).

[1] Note that single scattering is already a good approximation for twilight geometries

2 Retrieval strategy

We perform the DOAS analysis using QDOAS with settings outlined in FRM4DOAS-2.0:D8.1. In the reminder of this document, we will write DSCD to refer to the DSCD evaluated with a reference spectrum at the lowest SZA, unless otherwise stated.

2.1 Forward Model: Slant Column from vertical Profiles that are a function of local SZA

The Raditative Transfer Model (RTM), in our case DISORT wrapped inside `uvspec`, computes the modelled slant column by taking into account the profile at the local SZA, θ_l along the line of sight.

$$\mathrm{SCD}^{\mathrm{mod}}_{\mathrm{BrO}}(\theta) = \sum_{i=0}^{\mathrm{toa}} \mathrm{AMF}(z_i, \theta)\, n_{\mathrm{BrO}}(z_i, \theta_l)\, \Delta_z, \tag{1}$$

with $n_{\mathrm{BrO}}(z, \theta_l)$ the interpolated BrO number-density profile at θ_l and $\mathrm{AMF}(z_i, \theta)$ being the SZA and height dependent air mass factor in height bin z_i at SZA θ, and Δ_z the height of each bin, we use equi-distant height bins.

The BASCOE output are supplied to `uvspec` interpolated to the measurement SZAs (including the reference SZA). Apart from the SCD, `uvspec` performs a finite difference approximation to the Jacobian K, the BrO density is varied with a small amount in each layer height. This finite difference approximation makes the forward model computationally expensive.

If the supplied profiles x were not a function of SZA, then the linear approximation of SCD using the Jacobian K is simply:

$$\mathrm{SCD}^{mod} = K\, x \tag{2}$$

Performing one forward model simulation for each SZA BrO profile, we can test whether the linear approximation gives the correct SCD, we show these in Fig. 1, where each panel uses the fixed BrO concentration at a fixed SZA, as indicated in the panel title, for the complete range of SZAs.

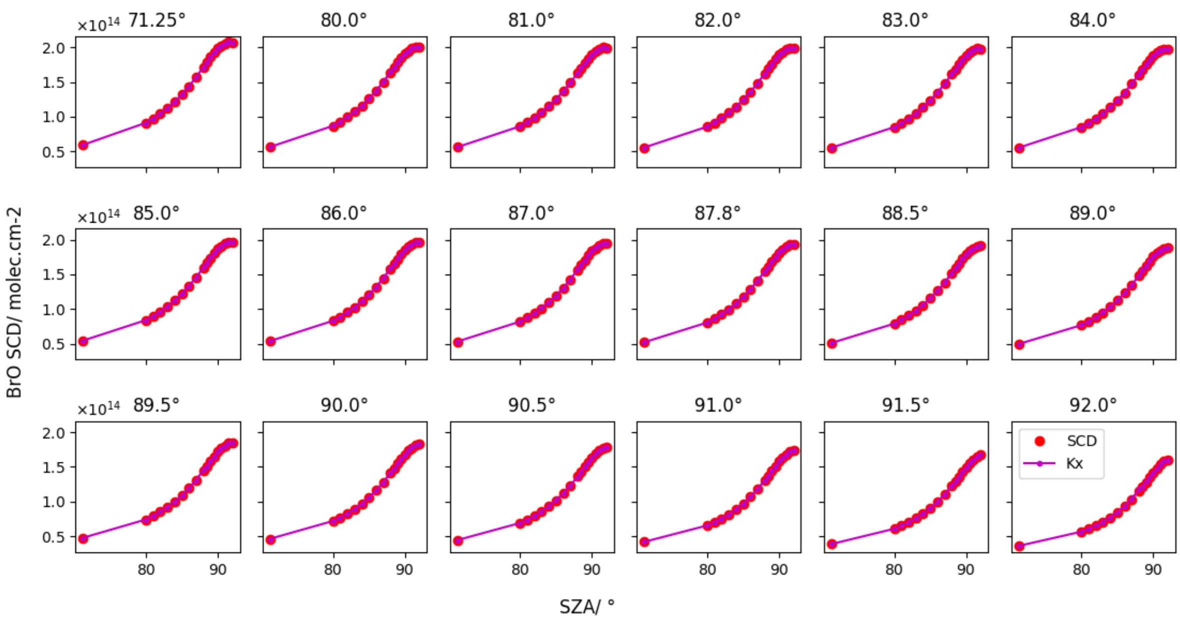

Figure 1: Simulated SCD (red circles) and the result of Eq. 2 (magenta line and magenta dots) when supplying BrO profiles to the forward model that are not a function of glssza. Each panel respresents a different fixed profile corrsesponding roughly to a simulated profile at the indicated SZA.

However, the actual profile x supplied to `uvspec` is not a 1D vector (function of height), but a 2D matrix, X, (function of height and SZA), therefore Eq. 2 becomes Eq. 3,

$$\mathrm{SCD}^{mod} = diag(K\, X) \tag{3}$$

We can test this by comparing the simulated SCD when supplying the 2D X to `uvspec` to the result of Eq. 2. In Fig. 2, we add this simulated SCD in each panel. Note that this is obviously the same curve in each panel. It is instructive to observe that for low SZA, the effect of local SZA is small and hence the two curves align in each panel at the given SZA. Once the local SZA along the los starts to deviate greatly from the SZA at the fixed site, the SCD using the profile varying with SZA starts to be larger than the SCD with fixed profile.

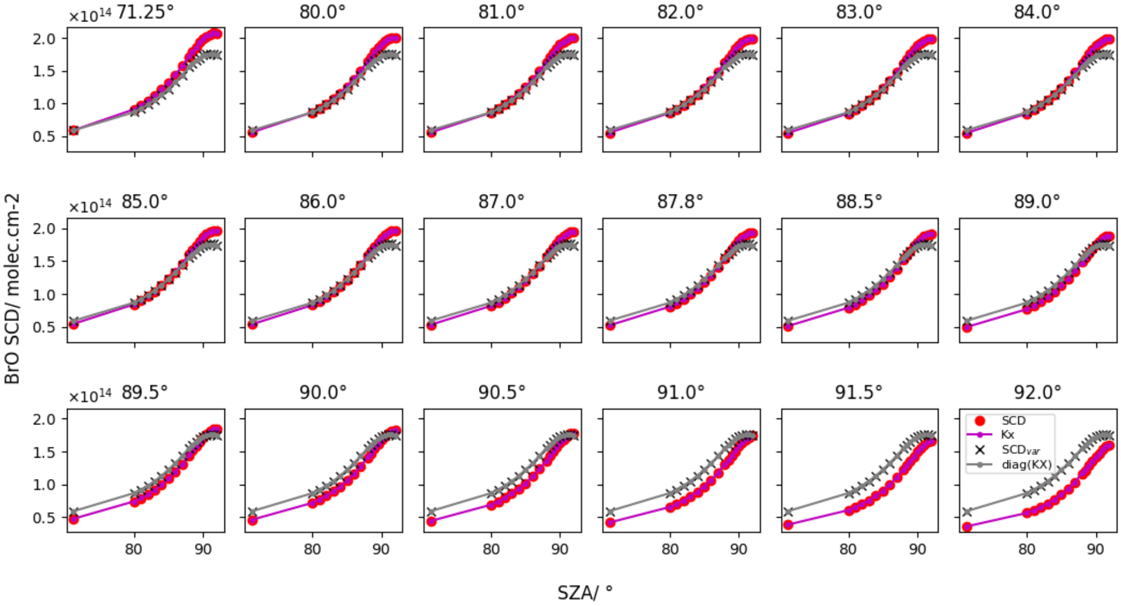

Figure 2: As Fig. 1, with added lines for simulated SZA using a profile varying with SZA (black crosses) and using the varying profile in Eq. 3 (gray lines and dot). Note that these are the same in each panel.

In a recent publication, Gomez-Martin et al. (2026) used Single Layer Isentropic Model of Chemistry and Transport (SLIMCAT) (Chipperfield, 2006a) in conjunction with integrating the SZA dependent profiles along the los and using Monte Carlo code for the physically correct tracing of photons in cloudy atmosphere (MYSTIC) RTM (Mayer, B., 2009) to get box-AMFs and SCDs. They compare their outcome to box-AMFs obtained from DISORT (Stamnes et al., 1988) embedded in a setup (modified `uvspec`) that handles the integration along the los taking the change of profile at different local SZA into account. They find reasonable agreement.

The forward model for differential measurements is

$$y = diag(KX - K_{\text{ref}}X) = diag(K_{\text{diff}}X), \tag{4}$$

with $K_{\text{diff}} = K - K_{\text{ref}}$.

2.2 Calculating the correct K

From Eq. 3, it is obvious that not a single profile x (e.g. x_a at the chosen retrieval SZA) can be used in Eq. 2 to reproduce the simulated SCD when supplying a SZA dependent profile. Hence, we need to account for the change in x as a function of SZA when using the Jacobian.

`uvspec` returns both K and the simulated SCD, $\text{SCD}^{sim}(\theta)$. We can define a $\widetilde{K}$ such that it fulfills Eq. 5.

$$\text{SCD}^{sim} = \widetilde{K}x_a = diag(KX) \tag{5}$$

where X is the 2 dimensional matrix of shape (heights, szas), the BASCOE BrO profiles at the measurement SZAs and x_a is the *a priori* profile at the chose retrieval SZA.

There are multiple possibilities for $\widetilde{K}$, e.g. the pseudo-inverse as in Eq. 6

$$\widetilde{K} = \frac{\text{SCD}^{sim}x_a^T}{x_a^T x_a} \tag{6}$$

or a solution that is closest to K (in terms of Frobenius norm[2]) that satisfies Eq. 5, as given in Eq. 7

$$\widetilde{K} = K + \frac{(\text{SCD}^{sim} - Kx_a)x_a^T}{x_a^T x_a} \tag{7}$$

[2]

$$\|A\|_F = \sqrt{\text{trace}\,(A^T A)}$$

, equivalent to Euclidian norm for vectors, (c.f. Horn et al., 1990) or a simple scaling as in Eq. 8,

$$\widetilde{K} = SCD^{sim}/(Kx_a)K \tag{8}$$

In Fig. 3, we show example Jacobians from evening twilight on 24 March 2003. Note however, that this is not K_{diff}, hence the corresponding weighting function at SZA_{ref} is also included.

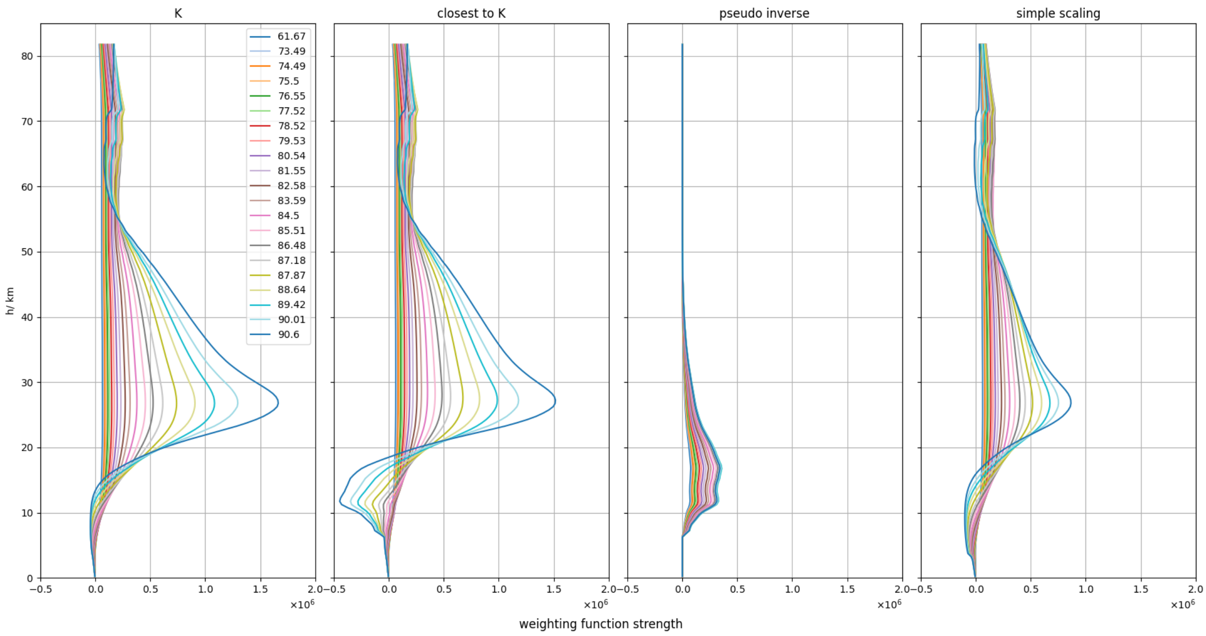

Figure 3: From left to right: Original weighting functions, closest to original weighting functions (in terms of Frobenius norm) that satisfies Eq. 5, pseudo inverse and weighting functions as a simple scaling, see Eq. 8. The SZA for each weighting function is indicated in the legend.

Tests showed that for the retrieval, whether using Eq. 7 or Eq. 8 to evaluate $\widetilde{K}$, has a negligble effect on the retrieved profile. We performed both approaches in all our investigations presented in Sect. 6. Since the differences are negligble, we only present results from the simple scaling, except for the example of the Averaging kernel (AK) in Fig. 12 where we also include the AK of the minimum Frobenius norm correction.

From Eq. 6 it is clear that a $\widetilde{K}$ calculated by a pseudo inverse contains no information about the actual simulated weighting function (while still satisfying formally Eq. 5) and hence should not be used in a meaningful retrieval.

2.3 Optimal Estimation Method Retrieval

In this section, when we refer to K, this refers to the corrected K, $\widetilde{K}$ as outlined in Subsect. 2.2. Further it should be understood that K is the differential K_{diff}. The BrO profile is retrieved by minimizing the Optimal Estimation Method (OEM) cost function (Rodgers, 2000) as given by Eq. 9

$$J(x) = (y - F(x))^T S_\varepsilon^{-1}(y - F(x)) + (x - x_a)^T S_a^{-1}(x - x_a), \tag{9}$$

where

- y is the measurement vector (DSCD as function of SZA),
- x_a is the a priori BrO profile at the retrieval SZA,
- S_ε is the measurement error covariance, in our case a diagonal matrix with the square of a multiple or fraction[3] of the DOAS DSCD fitting error on the diagonal.
- S_a is the a priori covariance, e.g. constructed as in Hendrick et al. (2004), where both the percentage of *a priori* on the diagonal as well as the correlation length to calculate off-axis elements are tunable parameters. More on alternative approaches for S_a are presented in Sect. 6.
- $F(x)$ is the forward model, in the linear case, this is $\widetilde{K}x$. As mentioned above, $\widetilde{K}$ is not the plane weighting function matrix returned by `uvspec`, but the corrected one obtained by Eq. 7 or Eq. 8.

[3]This multiplication factor constitutes a tunable parameter

The unrestricted OEM solution for the linear cases is then (c.f. Eq. 2.31 Rodgers, 2000)

$$\hat{x} = x_a + S_a K^T \left(K S_a K^T + S_\varepsilon\right)^{-1} (y - K x_a) \tag{10}$$

The averaging kernel matrix is

$$AK = \frac{\partial \hat{x}}{\partial x} = (K^T S_\varepsilon^{-1} K + S_a^{-1})^{-1} K^T S_\varepsilon^{-1} K, \tag{11}$$

which quantifies altitude sensitivity, vertical resolution, and dependence on the a priori.

The Degrees of Freedom (DOF) are

$$\mathrm{DOF} = \mathrm{Tr}(AK), \tag{12}$$

Instead of minimizing the cost function (Eq. 9) with an unconstrained linear approach leading to Eq. 10, we use a positive constrained minimization. Eq. 9 is mathematically equivalent to

$$J(x) = \left|S_e^{-1/2}(y - Kx)\right|^2 + \left|S_a^{-1/2}(x - x_a)\right|^2 \tag{13}$$

We can identify terms A and b to solve $|Ax - b|^2$ as

$$A = \begin{bmatrix} S_e^{-1/2} K \\ S_a^{-1/2} \end{bmatrix} \tag{14}$$

$$b = \begin{bmatrix} S_e^{-1/2} y \\ S_a^{-1/2} x_a \end{bmatrix} \tag{15}$$

Since S_e is strictly diagonal, $(S_e^{-0.5})_{i,i} = (1/S_{e_{i,i}})^{0.5}$. To compute $S_a^{-0.5}$, we first perform a Cholesky decomposition (using `cholseky` function from `numpy.linalg`, $S_a = LL^T$) and then apply `inv` from the same library to inverse L. For cases in which the requirements to perform the Cholesky decomposition fail (if Sa is not symmetric positive definite due to numerical issues), we create a new S_a from all Eigenvalues larger than 0.1% of the maximum of Sa and work with that. Finally, we can apply a posiitive restricted least square optimization to solve for x, we use `lsq_linear` from `scipy.optimize`.

In Fig. 4 we show an example for measured (black line in the left panel) DSCD from 24 March 2003 and *a priori* profile from BASCOE interpolated (black line in the right panel) at the measurement time closest to 80° which is taken as the retrieval SZA. We also show (right panel) the retrieved profiles applying the original K (yellow), the corrected $\widetilde{K}$ closest to K (cyan), the pseudo-inverse (green) and the simple scaling (magenta). In the left panel, with solid lines, we show the Kx_a with the same color scale. With circles, we show instead the modeled SCD applying `uvspec` to the retrieved profile that is translated to other SZA by applying the same time evolution as modeled by BASCOE but applied to the retrieved profile. As is evident from Fig. 4, applying the original K yields indeed a very good match between $\mathrm{DSCD}_{\mathrm{meas}}$ and Kx_a; however, applying actual forward simulations from photochemically adjusted profiles starting from the retrieval SZA and using the temporal evolution from the BASCOE simulations yields very different simulated DSCDs.

3 Chemistry

As argued in Hendrick et al. (2007), due to the rapid variation of BrO concentration at twilight, it is necessary to perform chemical model simulations, we choose BASCOE, see Subsect. 3.1. The most important chemical processes affecting the stratospheric BrO concentration during twilight are (e.g. Solomon, 1999; Stanley P. Sander et al., 2011; Wennberg et al., 1997):

- Br, BrO cycling:

$$\mathrm{BrO} + \mathrm{O_3} \rightarrow \mathrm{Br} + \mathrm{O_2} \rightarrow \mathrm{BrO} + \mathrm{O_3}$$

- Photolysis of BrO and $BrONO_2$:

$$\mathrm{BrONO_2} + \mathrm{h}\nu \rightarrow \mathrm{BrO} + \mathrm{NO_2} \qquad \mathrm{BrO} + \mathrm{h}\nu \rightarrow \mathrm{Br} + \mathrm{O(^3P)}$$

- Formation of gas-phase reservoirs:

$$\mathrm{BrO} + \mathrm{NO_2} + \mathrm{M} \rightarrow \mathrm{BrONO_2} + \mathrm{M}$$

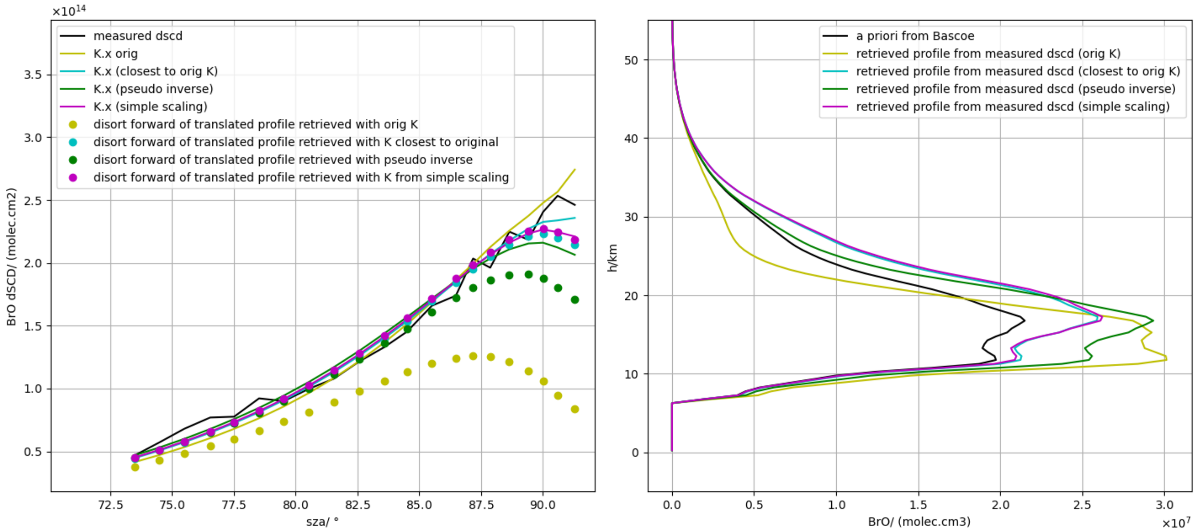

Figure 4: Left panel: measured (black) and DISORT simulated (circles, see legend for information on which profile was used in the forward model) as well as linear model implied (Kx_a) DSCD. Right panel: a priori profile and retrieved profiles using different expressions for the weighting function at 79.5° SZA. Note that the closest to original K (Eq. 7) and the simple scaling (Eq. 8), despite big difference in K yield very similar profiles.

3.1 BASCOE

BASCOE has evolved from a four-dimensional variational chemical assimilation (4D-Var) system described in Errera et al. (2001). It has since been constantly further developed and it has been used in many publications, e.g. in the framework of ozone inter-comparisons (e.g. Geer et al., 2006), for Michelson Interferometer for Passive Atmospheric Sounding (MIPAS) validation (e.g. Vigouroux et al., 2007). It is constantly updated to include more chemical processes (e.g. Vervalcke et al., 2025), updates of chemical rates (e.g. Chabrillat et al., 2025) as well as the option to use the ensemble Kalman filter (EnKF) approach as alternative to the 4D-Var (e.g. Skachko et al., 2016) as assimilation scheme.

For our purpose, we only use the CTM part of BASCOE without any assimilation scheme. We use BASCOE version 10 with chemical scheme `sb22d`.

The CTM simulates the temporal evolution of 57 stratospheric gas-phase species (Errera et al., 2008), accounting for advection, chemical and photo-chemical reactions, and the micro-physical processes of polar stratospheric cloud (PSC). The model is forced by wind and temperature analyses from meteorological centers, we use ERA5 reanalysis from European Centre for Medium-Range Weather Forecasts (ECMWF) (Hersbach et al., 2020). BASCOE's chemical scheme encompasses roughly 200 reactions, including gas-phase reactions, photo-dissociation processes, and heterogeneous reactions on PSCs.

In BASCOE, photolysis rates could be obtained by interpolating pre-computed Look-up table (LUT) that are generated offline as functions of log-pressure altitude, overhead ozone column, and solar zenith angle (Huang et al., 1998), but in our application we use online calculated photolysis rates. The underlying calculations rely on absorption cross-sections from published evaluations (JPL Evaluation No. 18 S. P. Sander et al., 2015).

BASCOE is a global model with a regular grid, we use a resolution (lon, lat) of (2.5°, 2°), i.e 91 latitude and 144 longitude points. The grid is a hybrid pressure-sigma grid, from orography following at the surface to equal pressure layer at top of atmosphere (toa). We use 61 pressure layers and the ERA5 toa of 1 Pa.

We use BASCOE as the forward model and extract the vertical BrO profiles at station locations at every time step. The time steps size Δt can be adjusted and the computation time scales linearly with the number of time steps N, where $N\Delta t$ corresponds to the total simulated time. In Fig. 5, we show the relation of computation-time and time-step-size.

Based on this, it seems feasible to perform daily global simulations with a 10 min time step, so simulating a full day takes about 20 min on 24 processors. In Fig. 6 we show examples of trace gas vertical profiles modelled by BASCOE for 24 March 2003. These profiles are interpolated at the measurement times of the DSCDs (and time of the reference spectra) and passed to the forward model.

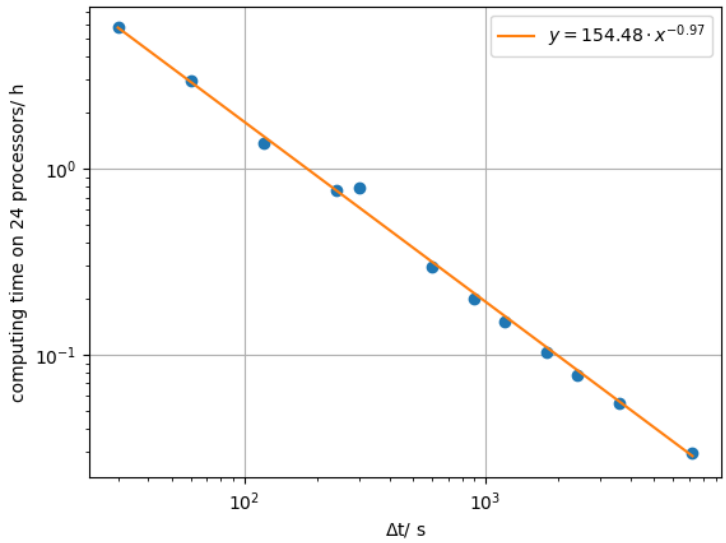

Figure 5: Relation between computational time and time step size Δt to complete 1 day of a global BASCOE simulation on 24 processors. Note that the computational time is also influenced by the load on the computational cluster; this explains the outlier at 300 s: This test was performed during a time where the compute servers were so busy that not always 24 processes could be used.

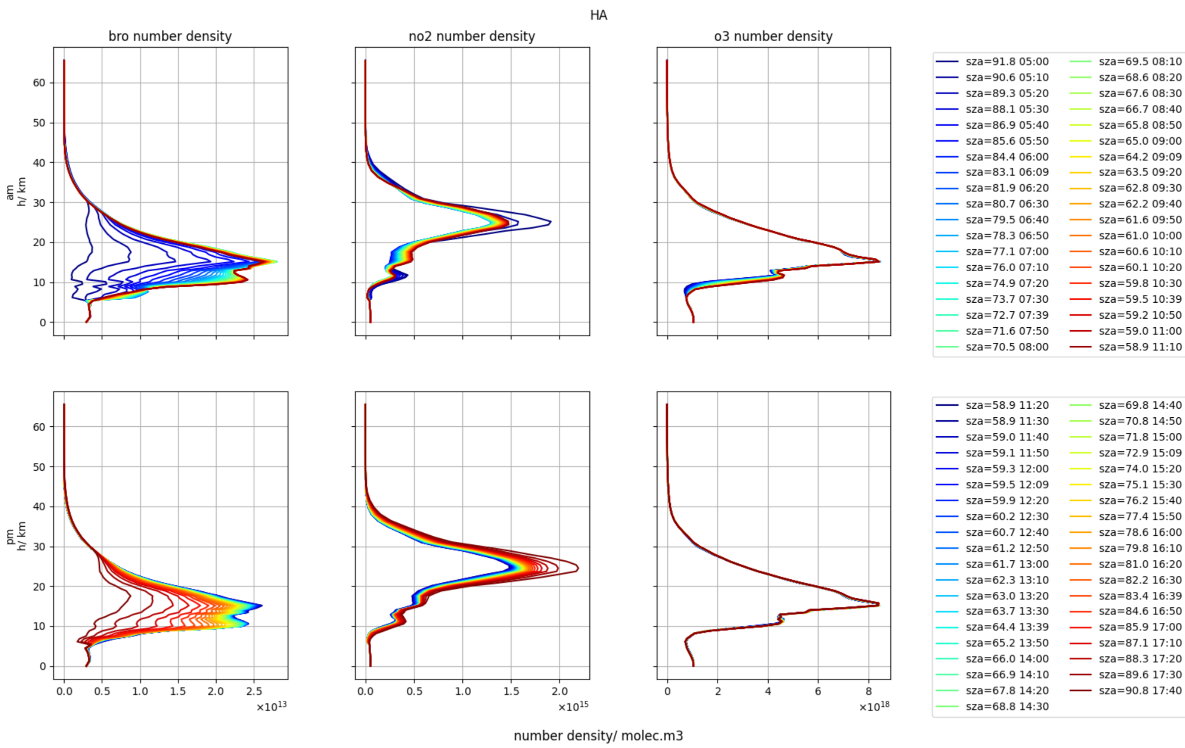

Figure 6: Example profiles modelled by BASCOE on 24 March 2003 of (left to right) BrO, NO_2 and O_3 for morning (upper panels) and afternoon (lower panels) times. Both the Coordinated Universal Time (UTC) as well as the SZA are indicated in the legend.

4 Forward model

For the forward model, we use DISORT (Stamnes et al., 1988) wrapped in a modified version of `uvspec` (Kylling et al., 2003; Mayer et al., 2005). The most important modification to use `uvspec` for BrO profile retrieval, consists in the addition of the ability to handle profile matrices instead of time (and SZA) constant profiles, so the second dimension of the profile matrix (the first being the height) is the SZA. As per the pseudo-spherical correction, the impact of the changing profile as a function of local SZA is only performed on the direct solar beam not on the diffuse multi-scatter part of the intensity.

This is no change compared to the model used in Hendrick et al. (2004), Hendrick et al. (2007) and Hendrick et al. (2008). It is also the same model used to create the LUT for the stratospheric NO_2 profiling package implemented in FRM4DOAS and described in FRM4DOAS:D6 and FRM4DOAS-2.0:D1.2.

It should be noted that we intend to use an altitude grid that is substantially finer than the ones used in the aforementioned publications, namely 0.5 km instead of 2 km. Additionally, the retrieval wavelength is chosen as 344 nm instead of above 400 nm (e.g. Hendrick et al., 2004), to represent better the center of the DOAS retrieval window.

Note that we found that for SZA=88°, `uvspec` seems to show some numerical instability. This was previously noticed during CCN-01 of the first FRM4DOAS contract already and interpolations were performed on the NO_2 LUT. For the work here that does not rely on LUT, care has to be taken of not requesting Jacobians too close to SZA=88°, compare Fig. 7. As is evident from Fig. 7, deviating by 0.2° seems sufficient to prevent this instability. Investigations of the cause of this instability are outside the scope of this Work package (WP).

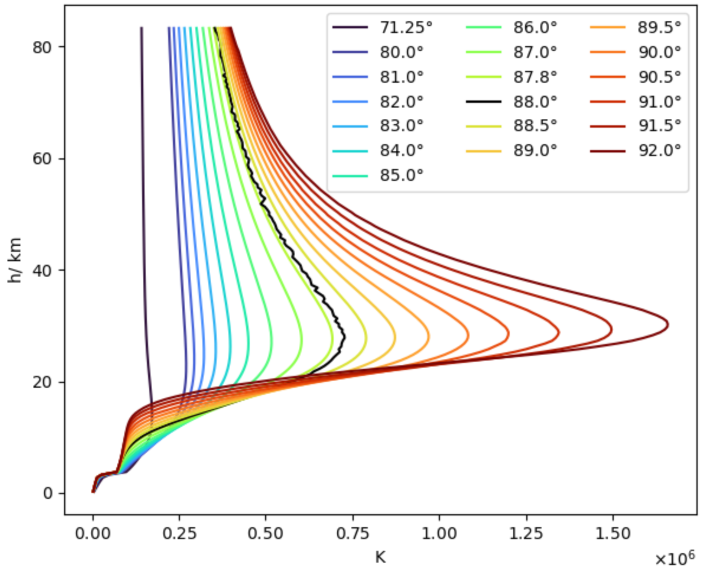

Figure 7: Demonstration of the numerical instability in the calculation of Jacobians around 88° SZA. Shown are the rows of the Jacbians as function of height, the corresponding SZA is color coded as shown in the legend. Note that for simplicity, this shows the Jacbians using a constant profile.

5 Differences w.r.t. stratospheric NO_2 as implemented in FRM4DOAS and BrO retrievals in the literature

As described in FRM4DOAS:D6 and FRM4DOAS-2.0:D1.2, the stratospheric NO_2 retrieval package of FRM4DOAS is based on LUT that use a two step approach instead of a single global CTM that includes photo-chemical processes on a relatively fine time scale: daily output of the 3-D CTM SLIMCAT (Chipperfield, 2006b) followed by a high time resolution photochemical 1-D box model, a part from PSCbox. While PSCbox, as BASCOE, evolved from the system outlined in Errera et al. (2001), it was not as consequently updated as BASCOE and is not any longer supported. Hence it was decided to change to BASCOE for the implementation of this work package.

The approach for the stratospheric NO_2 retrieval as outlined in FRM4DOAS:D6 and FRM4DOAS-2.0:D1.2 is based on LUTs, the CTM is run on several years and monthly averages are used for the LUT. As mentioned in Sect. 3, it is computationally still affordable to perform the BASCOE on a daily basis. Hence, we take advantage of the known atmospheric conditions, particularly whether a station is located inside or outside of the polar vortex. However, this also means that the RTM and the weighting function calculations need to be performed daily and, in contrast to the CTM, separately for each station. Effort was put in to be able to launch `uvspec` in a parallel manor from within python, making use of the ProcessPoolExecutor (part of the standard library), Python's high-level interface for running CPU-bound tasks using multiple processes. This ability is particularly important if we need to reprocess longer time series. For a single station, using 16 processes, we can process 1 year of data in just under 1 hour.

Note that while Hendrick et al. (2007) worked with absolute SCD, enabling also the possibility to retrieve tropospheric profiles, we plan to use DSCD and concentrate on stratospheric BrO, much as was done in Hendrick et al. (2008). Using DSCD is less prone to instrument degradation, as pointed out by Hendrick et al. (2008).

It should be also noted that while Hendrick et al. (2009) also uses daily reference DSCDs, they also constrain the photochemical model (used to translate the retrieved BrO to other SZAs than the retrieval SZA) using NO_2 profiles retrieved from simultaneous zenith-sky observations in the visible wavelength region. We are not planning to implement something similar in the operational approach since there is only one modeling step in the new approach.

6 Testing the implementation

The algorithm developed by F. Hendrick which was initially planned to be implemented in FRM4DOAS was previously used to produce Generic Earth Observation Metadata Standard (GEOMS) files of BrO stratospheric profiles for Harestua. These files were submitted to Network for the Detection of Atmospheric Composition Changes (NDACC). In order to validate our new implementation, the most logical step is to compare results obtained by our new implementation for a couple of years at that station to these existing results. The GEOMS data contain both profiles and averaging kernels, however, no simulated DSCDs are contained in the files.

For Harestua, there are also published stratospheric VCD obtained by a different method, using absolute SCD and using the tropopause height to divide the retrieved profile in a tropospheric and a stratospheric part. These results are published in Hendrick et al. (2007).

As a first step, instead of directly comparing our results to the above mentioned NDACC GEOMS files, we check for consistence of existing retrievals. Since we do not have access to the data in Hendrick et al. (2007), we extract the time series of sunset stratospheric BrO VCD directly from figure 10 of that publication and overlay the reported VCD from the GEOMS files. In a second step, we try to reproduce the settings used in F. Hendrick's retrieval as close as possible in terms of *a priori* profile and covariance matrix, S_a, retrieval grid, used SZA range, retrieval SZA and most likely choice to correct K. We present these comparisons in Subsect. 6.1.

In a second step, we exchange the *a priori* profile with data from BASCOE and follow the same approach to derive S_a. We then argue that the approach of deriving S_a directly from the used *a priori*, althogh often done in optimal estimation retrieval, is not recommendable. We present an alternative approach based on covariance from the RTM and compare the results of this new setup to the previously obtained ones in Subsect. 6.2.

While these sections only contain tests at Harestua using sunset retrievals, in Subsect. 6.3 we show results for sunrise retrievals and point out some striking differences. Subsect. 6.4 and Appendix A show results from three years (2002, 2022 and 2023) at Kiruna. Initially we also analyzed data for Lauder. However, we found large inconsistencies and investigations showed that these are due to a bug in the station extraction from BASCOE. While we have access to BASCOE source code, it is not within the scope of this project to fix the bug, re-do 3 years of simulations, reprocess the data and redo the analysis. However we note that the exercise we present below, helped us to discover the bug, this is briefly described in Appendix A

While we performed limited test of the effect of changing the range of SZA of measurements used for the retrieval, they are not presented since these tests were performed with the initial settings.

6.1 Reproducing NDACC results

In Fig. 8, we show the lower panel of figure 10 from Hendrick et al. (2007) which shows the retrieved stratospheric BrO VCD in red[4] retrieved at 80° SZA during evening twilight. We overlayed the stratospheric VCD from the above mentioned GEOMS files that were produced with a version of the algorithm we aim to implement, in blue. It is evident that the general agreement is fairly good, but each year, there are a few months in spring-early summer, in which the retrievals do not agree. Generally, the retrieval using the absolute SCD results is slightly higher stratospheric VCD during those months.

In order to reproduce the setting of the retrievals from the NDACC GEOMS files, we extract the *a priori* profile from those files. The profile used is only supplied for the retrieval SZA. We believe that this was 90° due to the order of magnitude of VCD and profile shape which resembles those of BASCOE at 90° SZA. We then express the *a priori* profile in the file, a, in terms of the BrO profile from BASCOE at 90°, b: $a(h) = f(h)\,b(h)$. We use this factor $f(h)$ to adjust the BASCOE profile at other SZA. Since we do not have access to the profiles at other SZA than the retrieval SZA, this is

[4] the original figure also included the troposheric VCD in black. In order to keep the plot clean, we deleted this in this reproduction

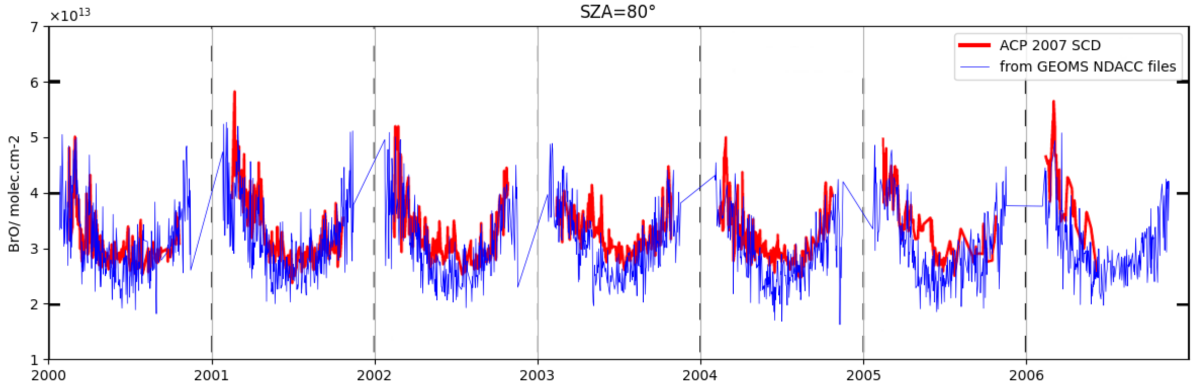

Figure 8: In red: reproduction of the lower panel of figure 10 from Hendrick et al. (2007) showing stratospheric BrO VCD retrieved during evening twilight at SZA 80° in Harestua. In blue: BrO stratospheric VCD from NDACC GEOMS files at 80°.

the only way for us to generate profiles at all SZA of the observations that were used for the retrieval. For SZA retrieval range we choose (80–93)° since this is the range used in Hendrick et al. (2009). We construct the covariance matrix used in the retrieval in the same was as in Hendrick et al. (2004), as used in Hendrick et al. (2008), namely using the square of a percentage of the *a priori* on the diagonal and constructing the off-diagonal elements as Gaussian functions using 8 km as correlation length.

As mentioned, while the retrieval in Hendrick et al. (2007) was performed at 80° SZA, the most likely retrieval SZA used in the retrieval of the NDACC GEOMS files is 90°. We perform the retrieval at 90° SZA and use a similar technique we used to translate the *a priori* profile extracted from the files to other SZA for the retrieval, to translate the retrieved profile to 80° SZAs. We show VCD at 80° and 90° in Fig. 9.

We can summarize the main results from this exercise as:

1. At 90° SZA, the stratospheric BrO VCDs of the new and original retrieval agree mostly fairly well.
2. At 80° SZA, where a distinct difference between the stratospheric BrO VCDs between the NDACC GEOMS files and the results from Hendrick et al. (2007) is present for late sprint/ early summer month, the new retrieval (translated to 80° SZA) tends to agree better with the results from Hendrick et al. (2007) than with the original retrieval from the NDACC GEOMS files.

As mentioned earlier, we are not able to fully reproduce the exact settings as used by F. Hendrick for the NDACC GEOMS files since we have only access to the *a priori* profile at 90° SZA and rely on BASCOE to translate this to other SZA. Hence, for days for which the CTM used by F. Hendrick and the one used by us differ, this translation will result in different profiles at SZA other than 90°. We should hence concentrate on a set of days for which we are able to reproduce the profiles best. In Fig. 10 we present 55 selected days during 2003 for which the new retrieved profile (in black) agrees to better than 10% in each height bins to the profile in the NDACC GEOMS files (in blue) when using the same *a priori* profile (in magenta), as extracted from those files. The date for each panel is indicated in the upper left in each panel. We also include the relative difference of the two sets of profiles (red dashed lines). Since the simulated DSCD is not included in the NDACC GEOMS files, in the reminder of this section, we consider the simulated DSCD of these close reproductions as the baseline.

Comparing closely the *a priori* to the retrieval in Fig. 10 reveals that the retrieval at low altitudes is often on, sometime below but never above the *a priori*.

Considering the DOF, a time series for Harestua during 2003 is shown in Fig. 11 and the AK, an example for Harestua on 2003-11-20 (pm) is shown in Fig. 12, shows that although the retrieval on this day (last panel in Fig. 10) is very similar (less than 5% difference in each altitude bin) and considerably different from the *a priori*, there are considerable differences in the AK and consequently on the DOF. The DOF only uses the trace of the AK to give an indication of the independent pieces of information of a retrieval. Note however that an AK that would indicate a shift between real profile and retrieved profile without any smoothing, would have a DOF of 0, since the information content of layer i in the retrieval about the real profile in layer i is 0. Hence we also show the full averaging kernels in Fig. 12.

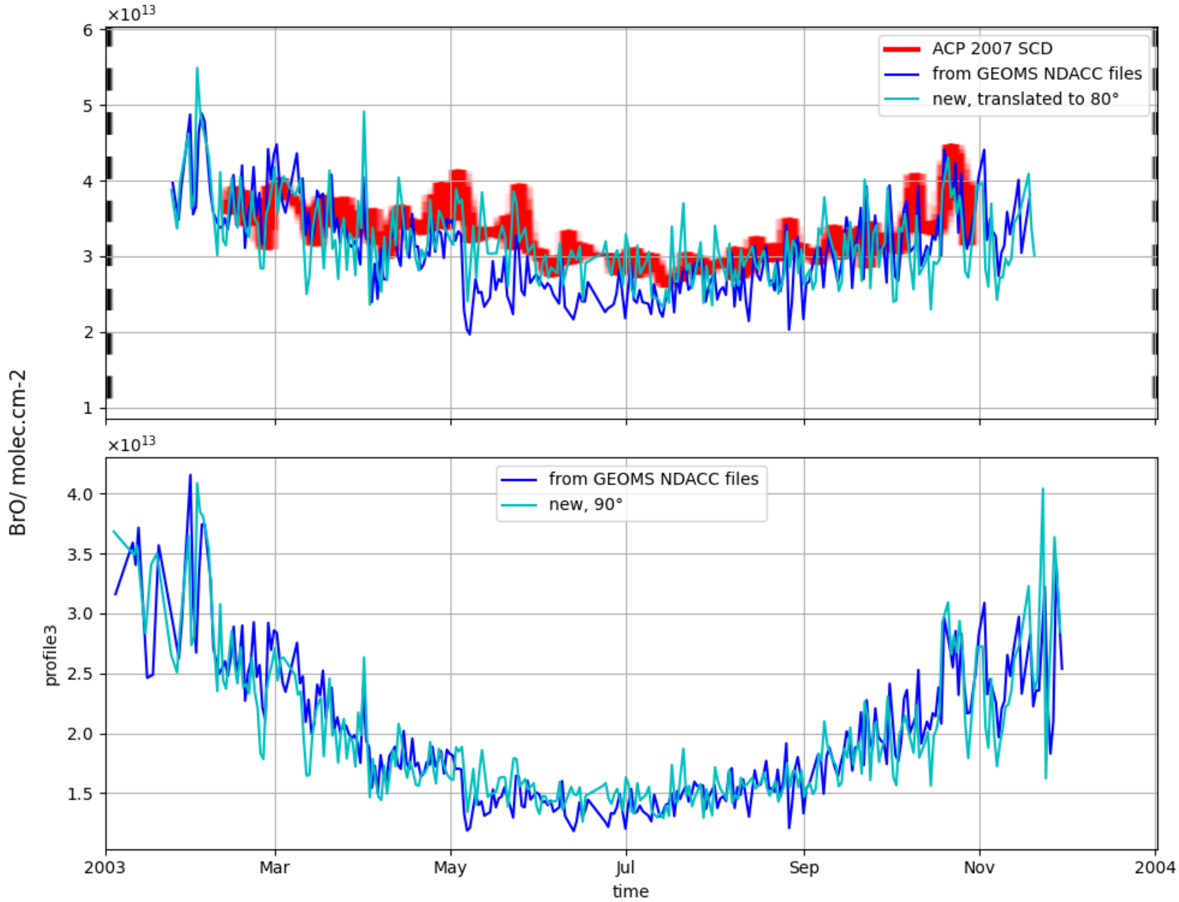

Figure 9: Stratospheric BrO VCD at sunset during 2003 in Harestua. The upper panel shows the VCDs at 80°, hence the data from Hendrick et al. (2007) is included. The lower panel shows the VCDs at 90°.

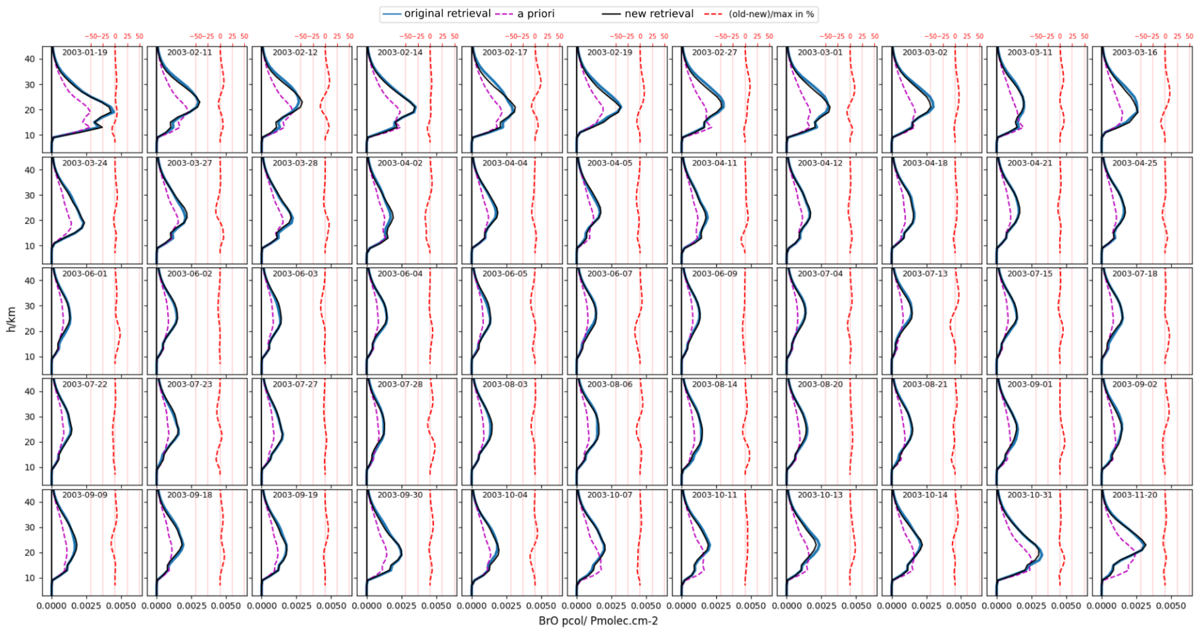

Figure 10: Selection of 55 days during 2003 (dates as indicated on the top left of each panel) showing both the original (from NDACC GEOMS files, in blue) and new retrieval (black) at Harestua using evening twilight measurements. In red, to be read with the upper x-axis tick labels, we show the relative difference between the two profiles in per cent. In magenta, the a priori at 90° SZA is shown.

The color scale was chosen such that it is symmetric around 0 and just covers the maximum (0.3) in each of the 3 panels. The AK in the original retrieval (left panel) however reaches highly negative values, more negative than -1. In general, the new retrieval also reaches fairly negative values, but mostly in absolute value not exceeding by much the maximum. The least negative contributions are found when applying the minimum Frobenius norm correction on K (right panel), compare Eq. 7.

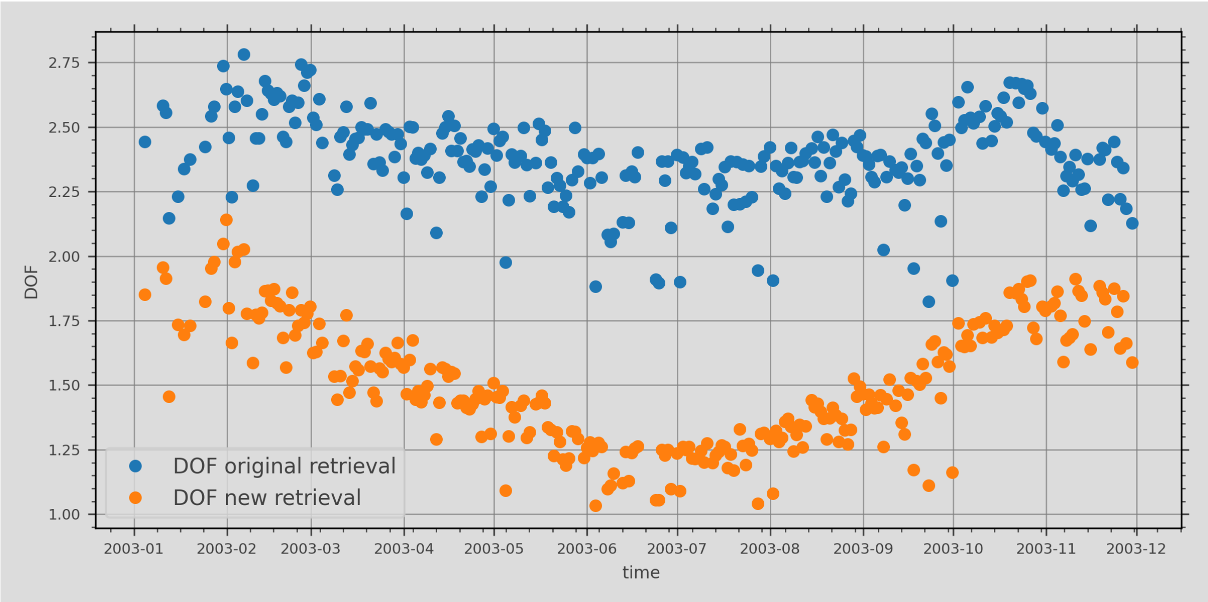

Figure 11: Time series of the DOF for 2003 at Harestua, evening retrievals. Note the large offset between the two

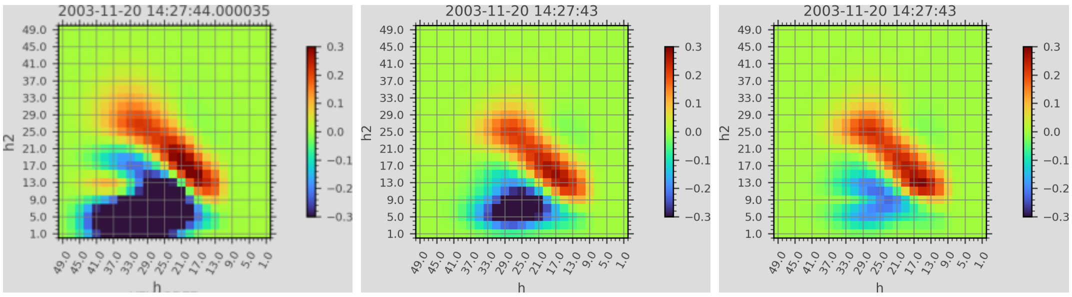

Figure 12: AK in vmr/vmr for the BrO retrieval in Harestua in the evening of 2003-11-20, from left to right: original retrieval, new retrieval using the simple scaling approach to adjust K (compare Eq. 8) and using the approach to stay as closely to the original K as possible (compare Eq. 7). Note that the color scale for the averaging kernel is chosen the same for all 3 panels. Note however that the original averaging kernel reaches values smaller than -1, while the minimum value for the new retrieval using the simple scaling reaches only -0.4.

Investigating the reason for the highly negative contributions in the original retrieval is outside the scope of this project. To conclude this part of the investigations, we can say that we are able to reproduce the profile retrieval on approximately 20% of days in 2003 for Harestua to a very high degree and for an additional 57% to some degree. As mentioned above, if the underlying chemical model between the old and the new retrievals were very different, we have no means to reproduce the original results. Hence, we believe that we are able to reproduce the original results for cases were the underlying chemical model had a similar diurnal variation of the BrO profile, and hence we succeeded in the implementation of the retrieval algorithm.

6.2 Exchanging a priori profile and covariance matrix

Our goal is to demonstrate that a switch to use BASCOE as the chemical model to provide *a priori* profiles at SZAs corresponding to all measurements used in the retrieval is valid. In order to do so, we concentrate on the previously selected 55 days at Harestua in 2003 and consider the evening retrievals performed at 90°. As outlined in the last section, we consider the simulated DSCD as our baseline. From these, we can calculate the Root mean square (RMS) of the difference between the measured and simulated DSCD and use this of an indicator how well our retrieval agrees with the measurements. Hence, beside comparing the retrieved profile, we also consider the change in RMS.

In Fig. 13 we show the original *a priori* which was already shown in Fig. 10, now in dashed blue, to the new *a priori* from BASCOE interpolated to 90° and with introducing a linear decay of concentration from 11 km to 9 km altitude. Additionally, a smoothing, applying a gaussian smoothing of 2 km length was applied in order to preven the effect of sharp double peaks from the coarse resolution of BASCOE.

As can be seen in Fig. 13, the underlying *a priori* profiles are often very similar. If they deviate, new profiles are generally a bit larger around 18 km, especially during the first 3 months. Additionally, even though a linear decay was applied, often the concentration around 10 km is higher.

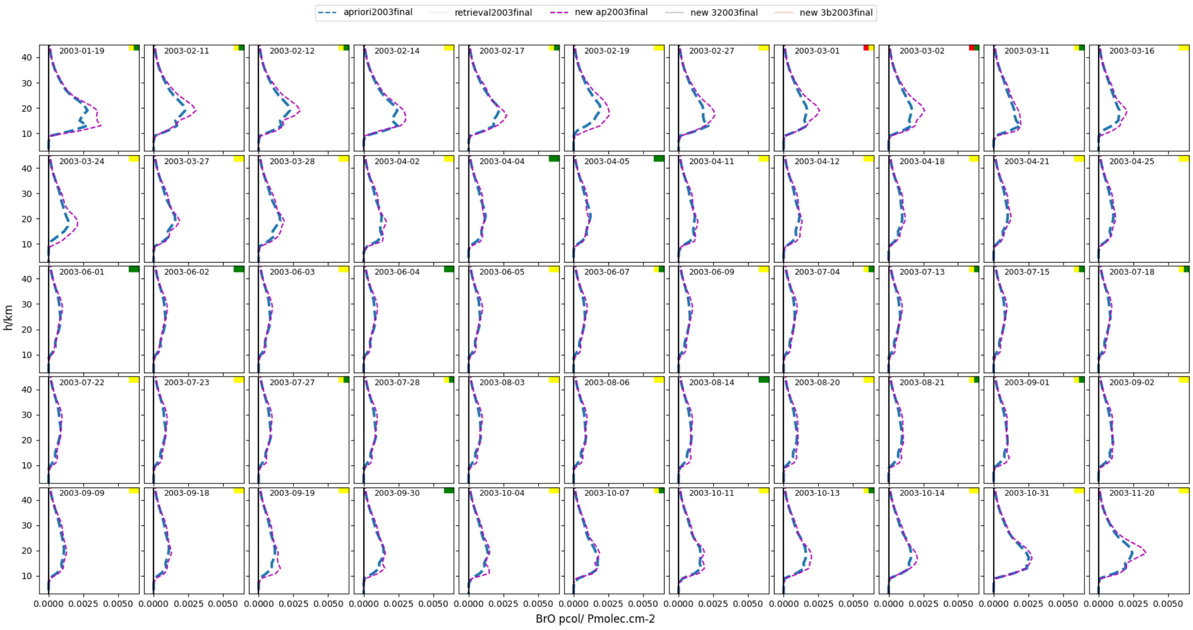

Figure 13: BrO a priori profiles used in the evening retrievals for the 55 days selected for Harestua in 2003. Shown are the old a priori profiles in dashed blue and the new a priori profiles in dashed magenta. The two colored squares in each panel are an indication of the change in RMS, for details, see main text

In Fig. 14 we show the retrievals for the same 55 days as the *a priori* profiles in Fig. 13. Included are the original retrievals from the NDACC GEOMS files (light blue), the retrievals using the new *a prioris* based on BASCOE profiles using the same approach to create the covariance matrix directly from the *a priori* profiles as outlined above (in black) and using a different approach that will be described later, in red. The colored squares in the upper right corner in each panel indicate whether the RMS improved (green) or deteriorated (red) by more than 10%, the first square in each panel represents the new retrieval with the S_a constructed from the *a priori* and the second square corresponds to the method that will be outlined below.

Overall, exchanging the *a priori* profiles to BASCOE based *a priori* profiles has a moderate effect both on the profile, and on the RMS. We show monthly means (using data from 2002 and 2003) of new and old *a priori* profiles together with monthly means of new and orginal retrievals in Fig. 15. The monthly means clearly show the previously mentioned larger concentrations in the new *a priori* profiles as well as the more distinct difference in late spring/ early summer months between the retrievals. While January also shows large differences, the overall number of retrievals is very low, less than 10, compare to approximately 50 – 60 in other months.

6.2.1 New approach to create Sa

As outlined above, the original approach to build the covariance matrix used the square of a fixed fraction of the *a priori* profile to build the diagonal elements of S_a. While not documented for BrO using differential slant columns, as presented e.g. in Hendrick et al. (2008), we believe that the used fraction was 30%. This is based on the fact that this value can be found in most code fragment versions of the initial implementation. In Fig. 16 we compare these assumed variance based on using the 25th percentile, median and 75% percentile in each month for Harestua (considering years 2002 and 2003) with the variance found in BASCOE simulations at evening 90° SZA. It is evident that the for most month, the order of magnitude of the maximum of the variance corresponds indeed roughly to that using 30% of the profile itself. However, it is also evident that in most month, the peak of the variance in BASCOE is in fact mostly at a lower altitude. Therefore, using the *a priori* profile to construct the covariance matrix will give freedom of variation at wrong altitudes.

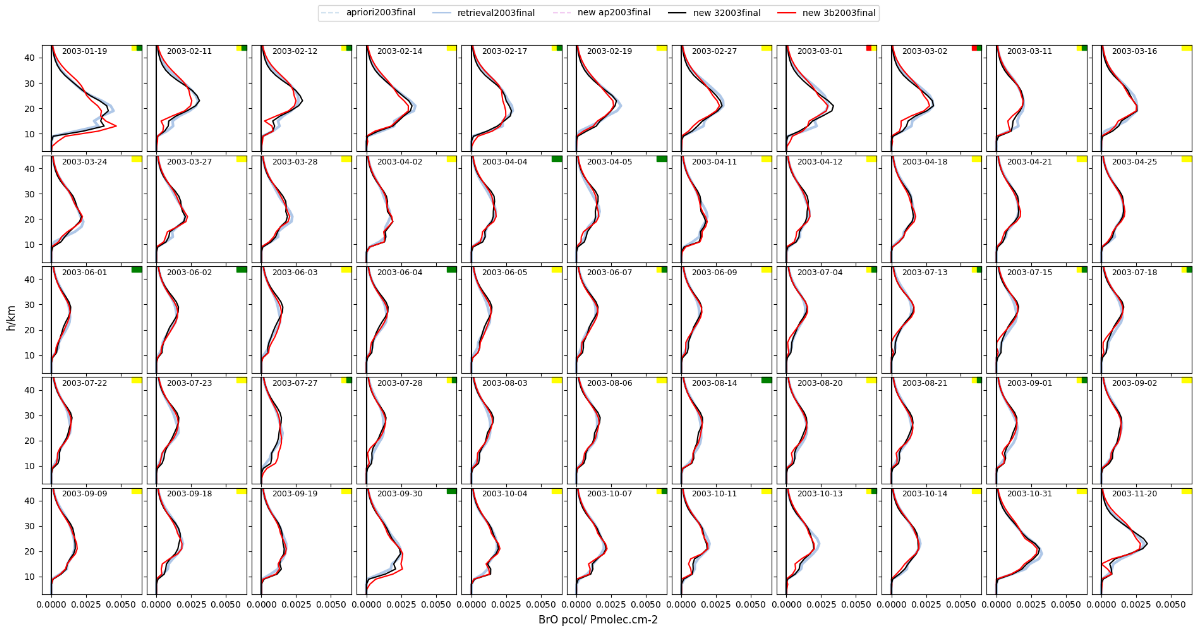

Figure 14: Retrieved BrO profiles corresponding to the a priori profiles presented in Fig. 13

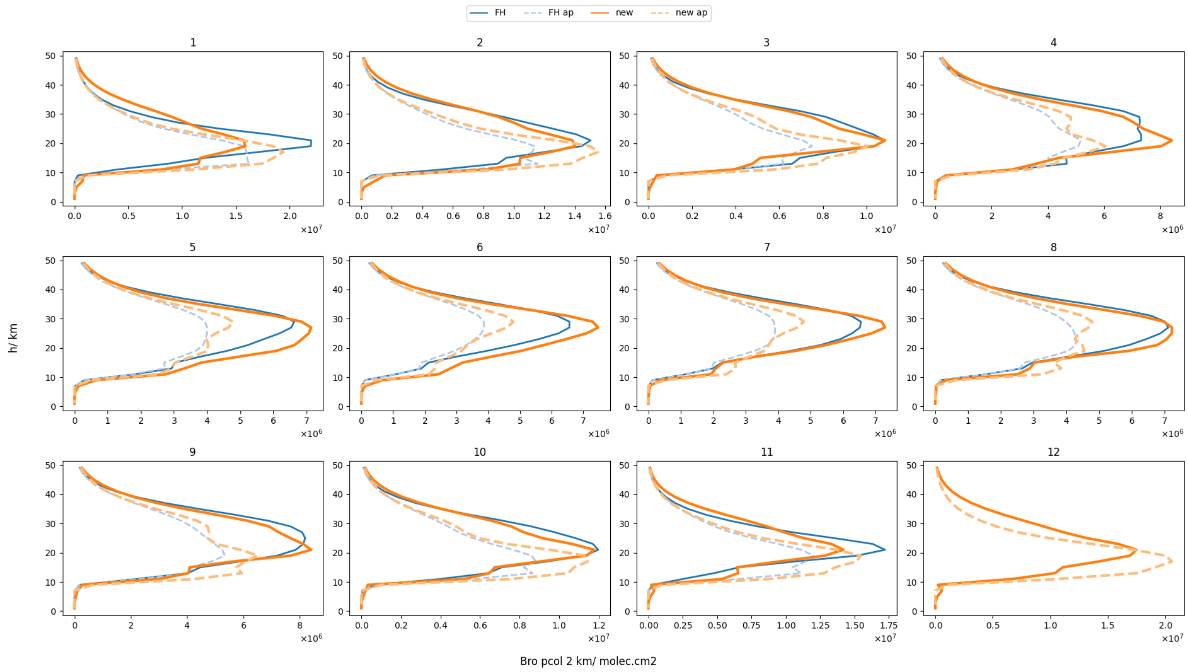

Figure 15: New (orange) and original (blue) monthly means (the month is indiated above each panel) of a priori (dashed lines) and retrieved profiles (solid lines)

Further, by using directly the varying (on a day-to-day basis) *a priori* to create S_a introduces a non-linear dependence. One effect is, for example in February, that the retrieval at altitudes around 11 km, in 25% of the cases (everything below the red line will have a diagonal elements in the S_a lower than this) cannot change from this low *a priori*.

As can be seen in Fig. 16, the variance from BASCOE is often peaked. While this might be physical, especially in winter, due to the occasional presence of polar stratospheric clouds, it is advisable to perform the retrieval with a smoother variance. Considering the covariance, these peaks also show off in the off-diagonal elements. Additionally, during summer month and late spring (e.g. May, June, July, August, last row in Fig. 16) the overall variance is very low. Additionally, the variance is very close to 0 at high altitudes. While all these might be physically correct, the simulated level of BrO concentration might still be incorrect.

Therefore, it is advisable to allow even at those times and altitude range, for some freedom in the retrieval and hence, for a non-negligible contribution in the S_a. Our approach is therefore:

- consider the variance from BASCOE at the chosen retrieval SZA in each month

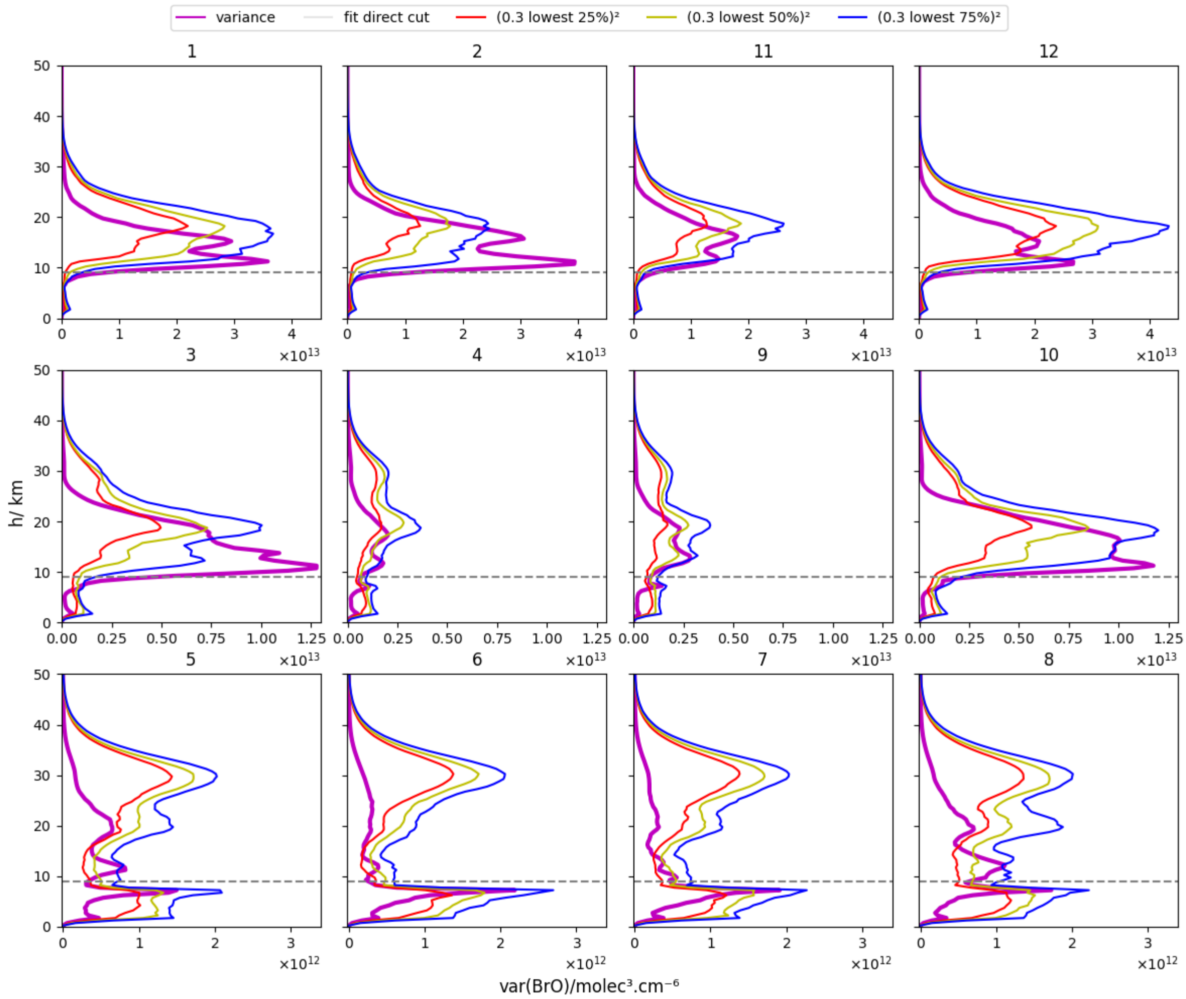

Figure 16: On a monthly basis, as indicated in the title of each panel, the variance of the profile in BASCOE in magenta. Also shown are created variances as they would be used in the S_a on days corresponding to profiles at the 25th (red), 50th (yellow) and 75th percentile. E.g. For January (first panel) this means that at 12 km altitude, the real variance is higher than estimated in 75% of the retrievals.

- consider the variance constructed from the 5th percentile
- use the maximum of these as a baseline for the variance at each altitude level in each month
- fit the so-constructed curve with a skewed gaussian
- use the approach of gaussian functions of 8 km Full Width at Half Maximum (FWHM) to construct off-diagonal elements
- consider these as representative S_a for the middle of each month and perform a linear interpolation for the retrieval day

The first 4 steps of this approach are illustrated in Fig. 17 as an example for May in Harestua at 85° SZA

6.2.2 VCD comparison

With these changes in place, we can re-do the VCD comparisons shown in Subsect. 6.1. Besides the profile and stratospheric VCD at 80° and 90° SZA, the NDACC files also contain these values at 85°, wherefore we also include that wavelength in the tests of this section. In Fig. 18 we show a subset of years (2002 and 2003) of what was shown in Fig. 8 in the middle panel. Additionally, we add stratospheric BrO VCDs from the new retrieval performed at different SZAs, all translated to 80° SZA. Since the retrieval performed at 90° SZA has a higher day-to-day variation than retrievals performed at other SZAs, we also plot a 4-day average to make comparison easier. Concentrating on this panel, it is evident that all new retrievals, independent of the chosen retrieval SZA, agree reasonably well with both retrievals from F. Hendrick. Further it is visible that the new retrieval

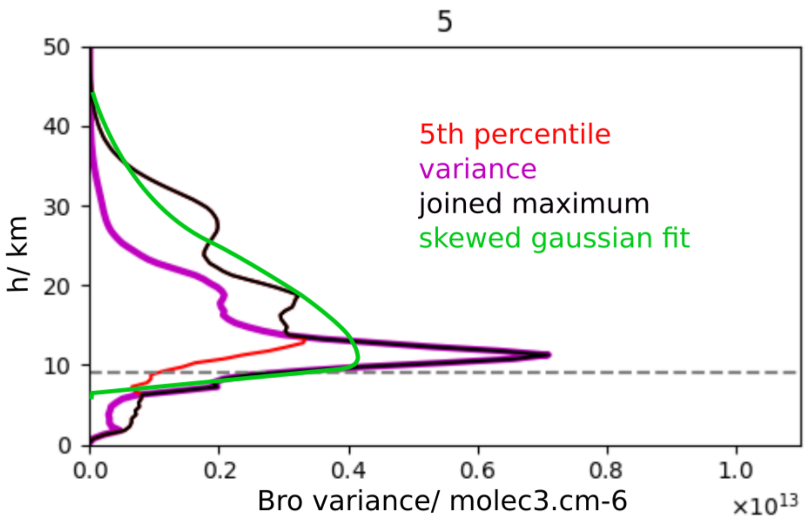

Figure 17: Outline of proposal how to create diagonal elements of S_a, here for Harestua sunset in May.

agrees better with the retrieval based on the absolute SCD presented in Hendrick et al. (2007) in the month in which that retrieval deviate from the results in the NDACC GEOMS files. This is the same result as already found in Subsect. 6.1 when applying the same settings as presumably used in the production of the NDACC GEOMS files. The remaining two rows show stratospheric BrO VCDs at 90° (upper panel) and 85° (lower panel).

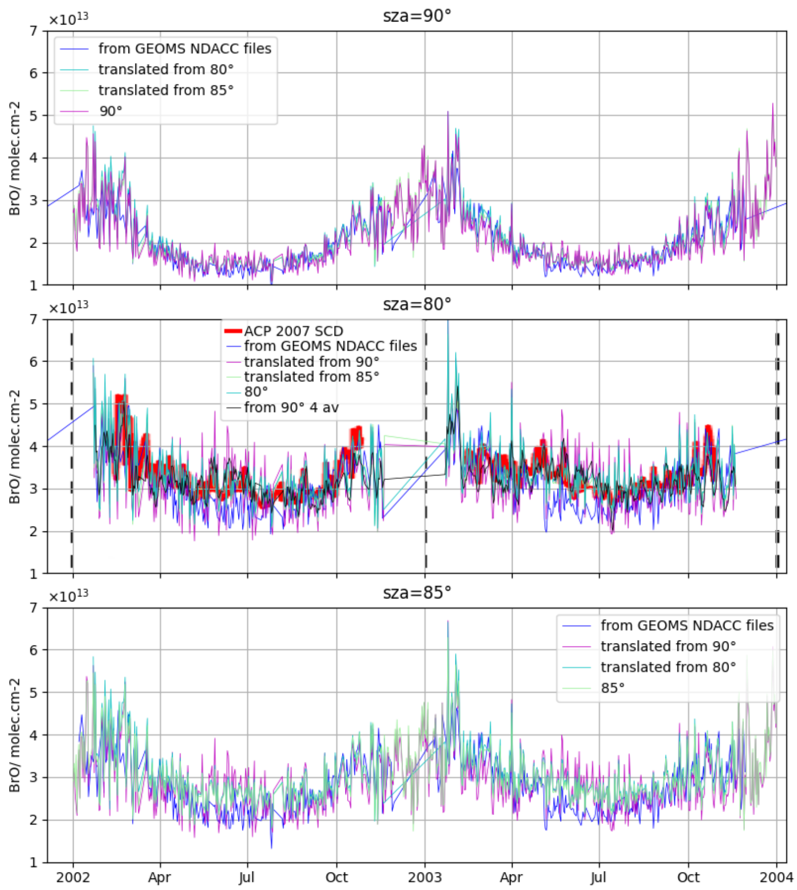

Figure 18: The middle panel shows a subset of 2 years from Fig. 8, 2002 and 2003, the stratospheric BrO VCD at 80° SZA at evening twilight. Added to the previously shown 2 curves representing different versions of retrievals performed by F. Hendrick, we add 3 curves representing new retrievals performed at different SZAs translated to 80°. Additionally, as the last curve in black, we add a 4 day average of the 90° retrieval translated since it is very noisy. The other two panels show the retried VCD at other SZAs as indicated in the title.

6.2.3 Detailed profile investigations

In Fig. 13 (*a priori*) and Fig. 14 (retrieved), we showed 55 selected days including both the original and the two versions (*a priori* based S_a and simulation variance based S_a) of the new retrieval. In Fig. 19 we show only 6 evenings during summer of these, combining all curves in each panel. It is evident that the *a priori* vary only moderately, the new having higher concentrations, both at lower and higher altitudes and very similar ones around 20 km. For 4 of the days (all but 2003-07-27 and 2003-07-28), the RMS between the measured and the simulated DSCD is very similar, meaning that the retrieved profiles are all equally consistent with the measurements. Observing the profile at low altitudes closely, it can be seen that both the original retrieval (blue solid line) and the new retrieval applying the same S_a creation strategy (black solid line), both follow their respective *a priori* closely. However, the new retrieval using an S_a build using BASCOE variances, and hence having considerable higher values at low altitudes), is below its *a priori* and is in fact closer to the original retrieval.

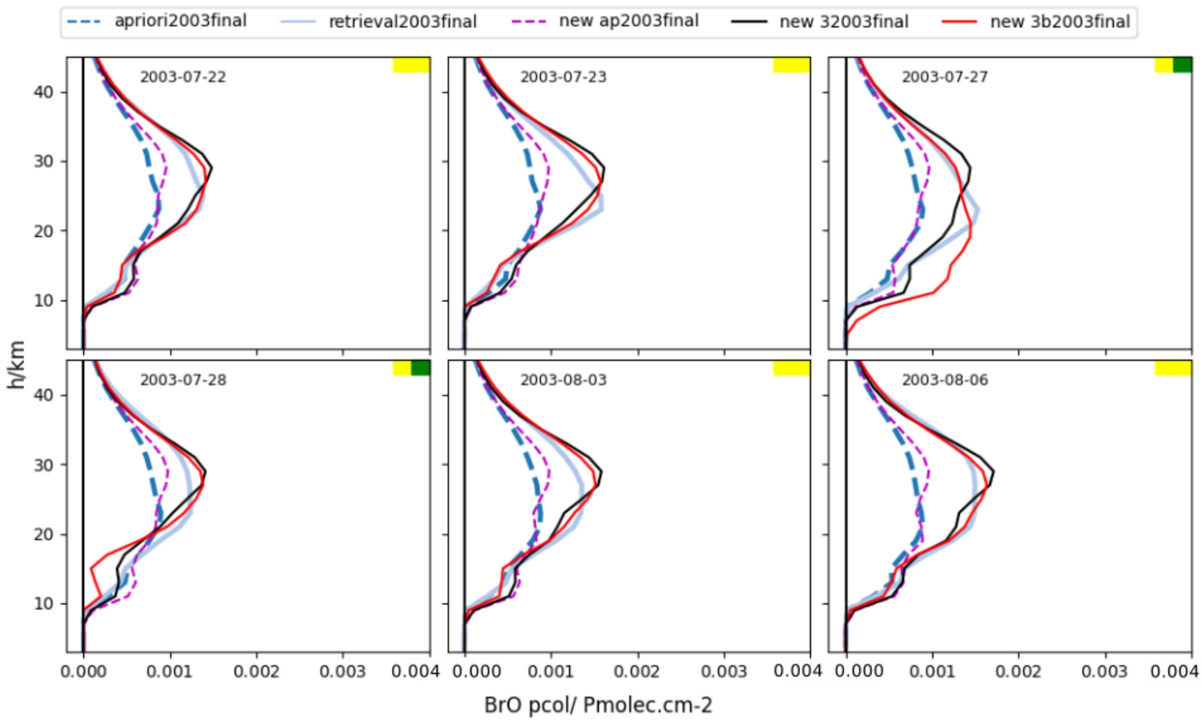

Figure 19: Retrieved profiles and a priori profiles from 6 evenings during summer in 2003 at Harestua at 90° SZA

On the remaining two days, 2003-07-27 and 2003-07-28, the new retrieval has a distinctly different profile shape. ERA5 reanalysis data (c.f. Fig. 20) shows the onset of a very strong (of the order of 50 m/s) S-W jet-stream at about 10 km altitude the late evening of 2003-07-27, likely strongly influencing the BrO concentration just around sunset, transporting BrO rich airmasses eastwards. The wind direction changes towards S in the evening of 2003-07-27, having likely the opposite effect, since sunset happens slightly earlier towards the south. These dynamics are not represented in the rather coarse (in time and spatial dimension) BASCOE simulations. While the new retrieval with the new approach to construct S_a results in lower RMS, the resulting profiles are equally questionable than the other retrieved profiles on that day. Since our chemical model cannot account for these small scale and likely very restricted in time effects, ideally, these retrievals should be flagged as invalid.

We can build S_a matrices following the above mentioned procedure at any SZA in order to perform the retrieval at a range of different SZAs. We can then use the above outlined approach (of using BASCOE profile) to translate the retrieved profile to all SZAs and compare the consistence of the retrieval. In Fig. 21 we show this for 2003-09-07 as an example where the retrieval is very consistent and largely independent of the choice of retrieval SZA. Each set of panels contains two panels, once the profile (left) and once the VCD. Each set of panels corresponds to the retrieved profile translated to a different SZA as indicated in the top left of each set of panels. Each panel contains retrievals performed at all SZA according to their color, see legend. We include uncertainty based on the smoothing and noise error as defined in Rodgers (2000), only for the retrieval where the SZA the profile corresponds to (as indicated in the panel), coincides with the retrieval SZA (as indicated by the color). It is evident that for all SZAs the retrievals performed at any SZA lies within these uncertainties. Similarly, it can be seen that the VCD is very stable when considering it as a function of retrieval SZA (right panel in each set of panels).

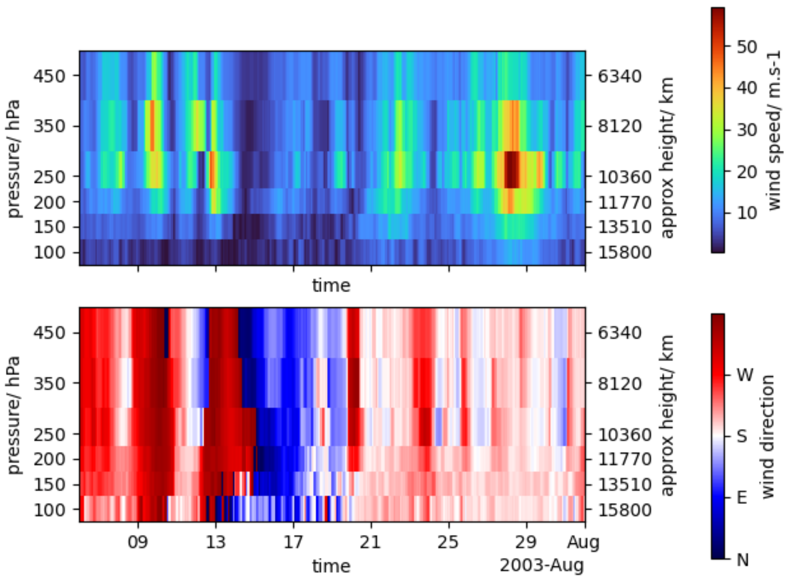

Figure 20: Wind speed (upper panel) and wind direction at Harestua during July, 2003

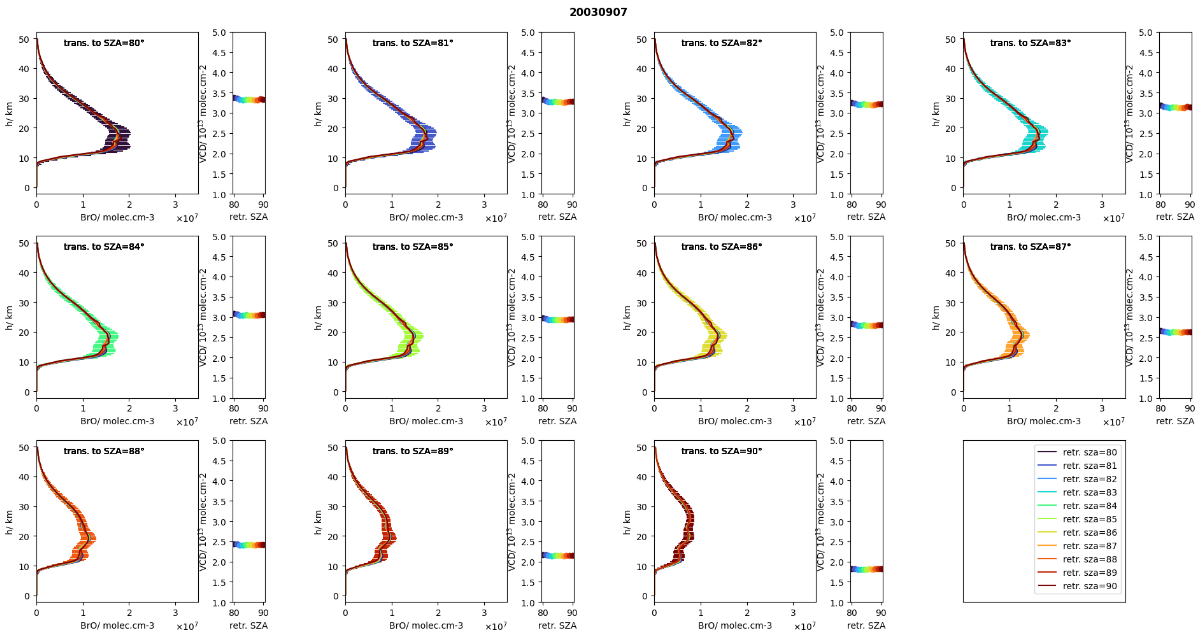

Figure 21: Retrieved profiles (left panel of each set) and stratospheric VCD for Harestua in the evening of 2003-09-07 at different SZAs as indicated in each set of panels. Each panels shows retrieved quantities from retrievals performed at different SZAs as indicated in the legend.

Considering instead one of the two days for which the new retrieval profile deviated substantially from the NDACC GEOMS profiles, as well as from a retried profile using BASCOE for the *a priori* profile but constructing the S_a in the standard way, shows larger differences. Fig. 22 shows the same type of plot as Fig. 21, but for 2003-07-27. This is the day on which a strong S-W jet stream onset happened just around sunset at about 10 km altitude (c.f. Fig. 20). It is clearly visible that the profile retrieval at 90° SZA is outside the uncertainty range at some altitudes at almost all SZAs. We conclude that the real change of BrO profile, likely due to the transport of BrO richer air transported via the jet-stream at about 10 km altitude, yields an unexpected SZA dependence of the profile and hence does not fit the CTM that the retrieval is based on. Likewise, the VCD as a function of retrieval SZA is not stable but increases steeply with retrieval SZA.

Concentrating on the VCD, we can show the VCD at 85° SZA both as a function of time and retrieval SZA. We show this in the left panel of Fig. 23. However, since the change of VCD over the course of the year is much larger than the possible inconsistencies between different retrieval SZA, we show in the right panel of the same figure the fractional change at each day compared to the minimum VCD of each day. E.g. at the beginning of March, there is a day where the retrieved VCD

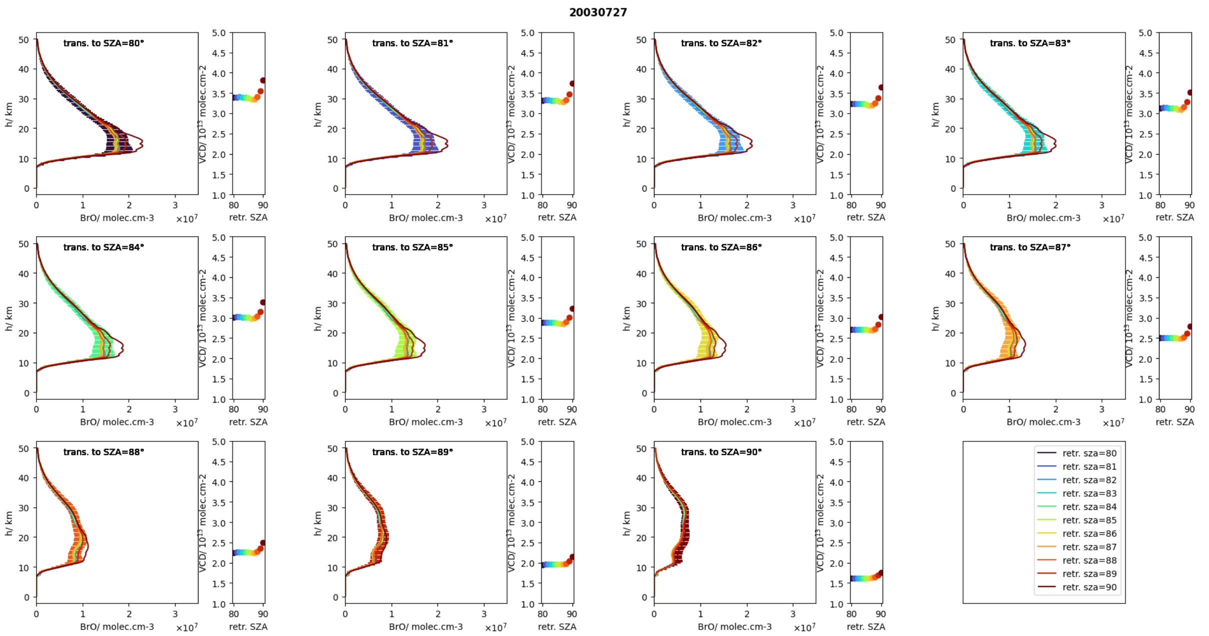

Figure 22: As Fig. 21 but for 2003-07-27

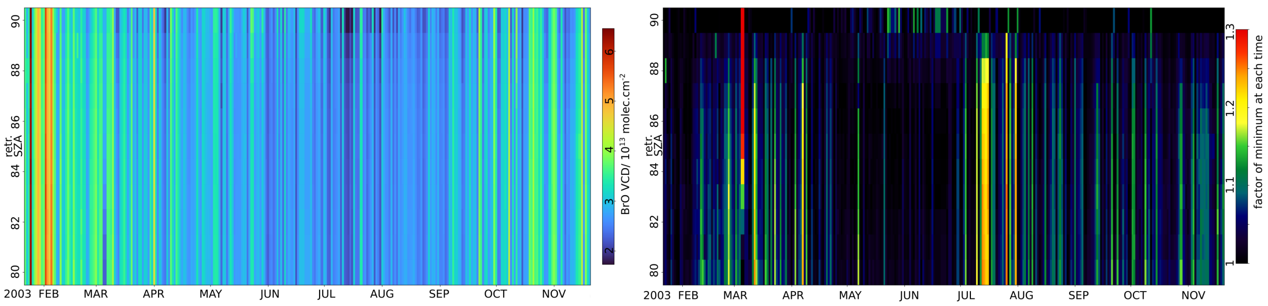

Figure 23: Left panel: Retrieved evening stratospheric VCD at 85° SZA (color scale) as function of day of year (x-axis) and retrieval SZA (y-axis). Right panel: fractional change of VCD compared to the minumum retrieved VCD on each day as function of retrieval SZA.

changes 30% depending on the chosen retrieval SZA; the smallest VCD at SZA 85° is retrieved when using 80° as the retrieval SZA and the largest when using 90° as the retrieval SZA. It is evident from the right panel of Fig. 23 that the variation of retrieved VCD with retrieval SZA is generally below 15% and often smallest at 90° retrieval SZA.

We conclude from this exercise that performing the retrieval at different SZA, one being 90° and the other lower, possibly 85°, is a way to check the internal consistence of the retrieval and can be used, additionally to the RMS as a way to filter for invalid retrievals.

6.3 Morning retrievals at Harestua

Until now, only evening retrievals were considered. While we have not performed all the tests as performed for evening retrievals, it is instructive to compare the two different retrievals from F. Hendrick also for the morning retrievals, as was done in Subsect. 6.1 and Subsect. 6.2.2, the latter including the new retrievals.

For the evening retrievals, our findings presented above, can be summarized as follows:

1. The VCD from the NDACC GEOMS files agree reasonably well with the data from Hendrick et al. (2007)

2. Between these two datasets, there is a larger difference in late-spring/ early summer month, the VCD in Hendrick et al. (2007) being generally larger

3. The new retrieval agrees reasonably well with both, for early-spring/ late summer, the agreement with the data from Hendrick et al. (2007) is better.

4. Mostly, the VCD is independent of the retrieval SZA

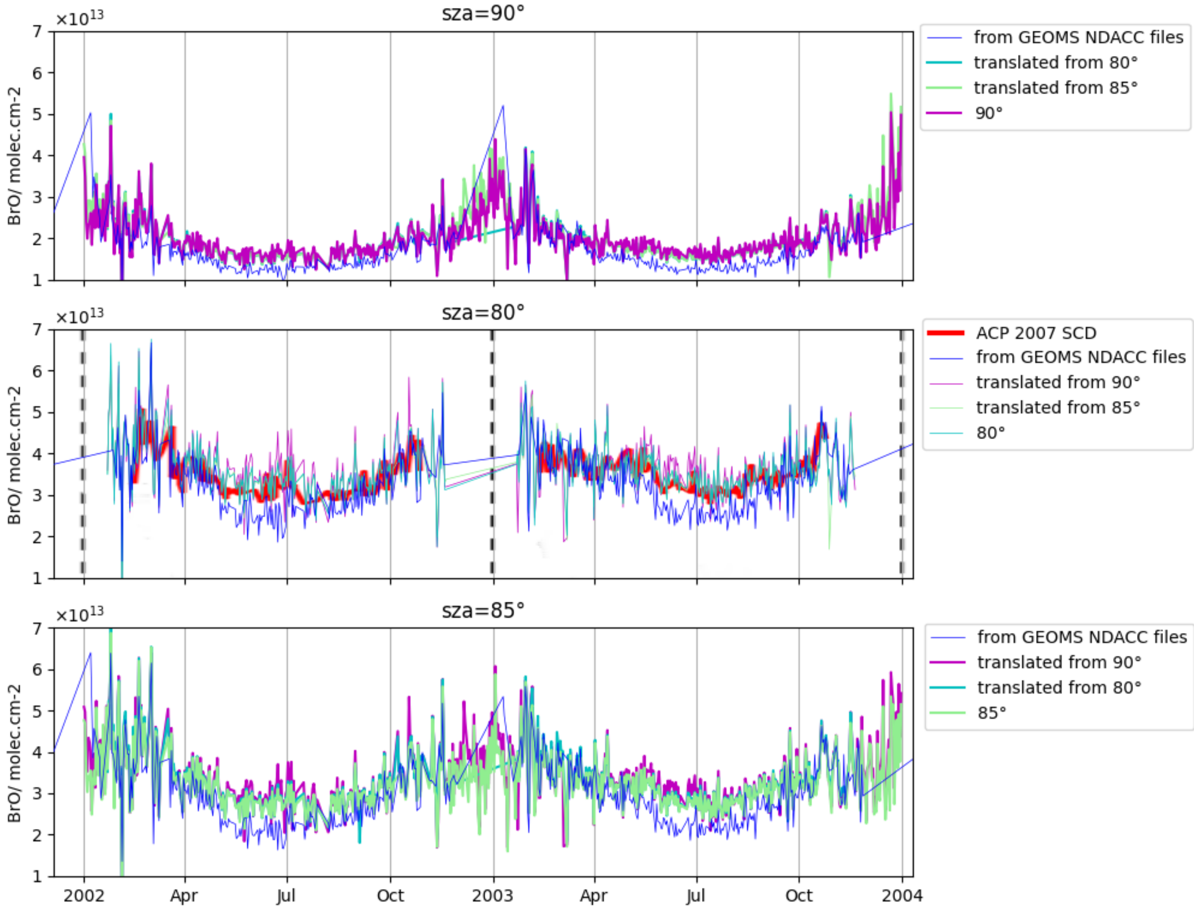

Figure 24: As Fig. 18 but for morning retrievals.

In Fig. 24 we show a similar plot as was shown for the evening retrievals in Fig. 18, but now for the morning retrievals. It is evident that from the list of findings above, the difference listed under 2, is even more pronounced and extends to mid-summer. The new retrieval still agrees better with the data from Hendrick et al. (2007) during these months than with the data from the NDACC GEOMS files. The difference between the NDACC GEOMS files and the new retrievals in summer, previously mostly seen ad 80° SZA is now also seen at 90° SZA.

We found for evening retrievals that, except for a larger scatter when performing the retrieval at 90° SZA, no systematic change could be found. We can plot the translated VCD retrieved at 80° and 85° SZA to 90° SZA over VCD retrieved at 90° SZA, as in the left panels of Fig. 25 (other panels show the same but translated to SZA as indicated). Both evening an morning retrievals seem to show no systematic effects w.r.t. the choice of retrieval SZA.

Finally, limiting to profiles at 85° SZA retrieved at 80°, 85° and 90° retrieval SZA, we can investigate whether there are systematic changes in the retrieved profile. We present the absolute differences $Delta(A, B)_{\mathrm{abs}}$ and relative $Delta(A, B)_{\mathrm{rel}}$ as defined by Eq. 16 and Eq. 17, respectively, between retrievals $p(A, A)$ performed at retrieval SZA A at SZA A and those profiles $p(A, B)$ performed at retrieval SZA B and translated to SZA A for $A = 85$ and $B = 80$ as well as $B = 90$ in Fig. 26 for absolute differences and relative differences Fig. 27. It is instructive to compare this to the combined uncertainty from smoothing and noise error, we show this is Fig. 28 for the retrieval at 85° SZA.

$$\Delta(A, B)_{\mathrm{abs}} = (p(A, A) - p(A, B) \tag{16}$$

$$\Delta(A, B)_{\mathrm{rel}} = 200\,((p(A, A) - p(A, B))/((p(A, A) + p(A, B)) \tag{17}$$

It is evident that frequently, the estimated uncertainty from smoothing and noise error is in fact smaller than the difference between retrievals performed at different retrieval SZA.

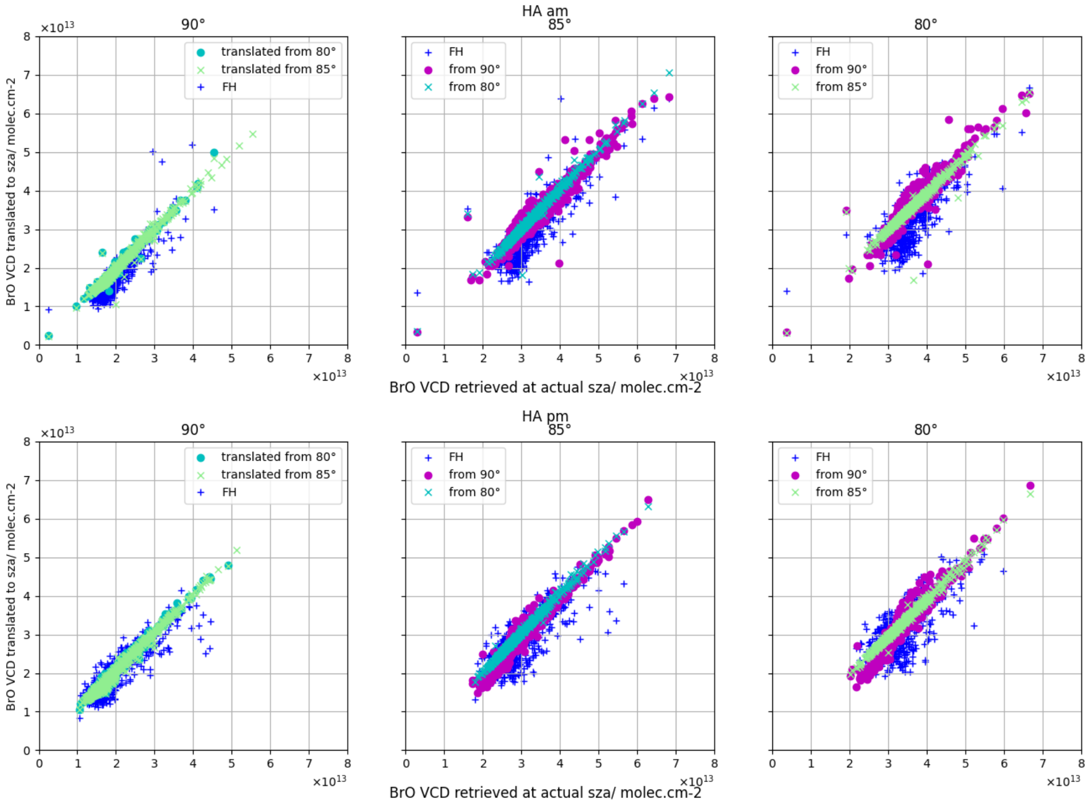

Figure 25: Scatter plots showing for 3 different SZA (left to right: 90°, 85° and 80°) the VCD of a retrieval translated to that SZA over the VCD performed at that SZA for Harestus, top panels for sunrise retrieval, lower panels for sunset retrievals.

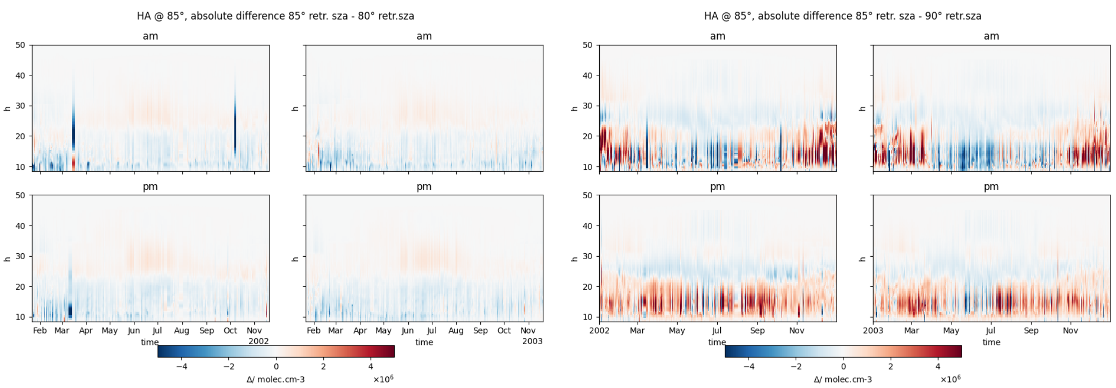

Figure 26: Absolute difference as defined in Eq. 16 for A=85° and B=80° (left) and B=90° (right)

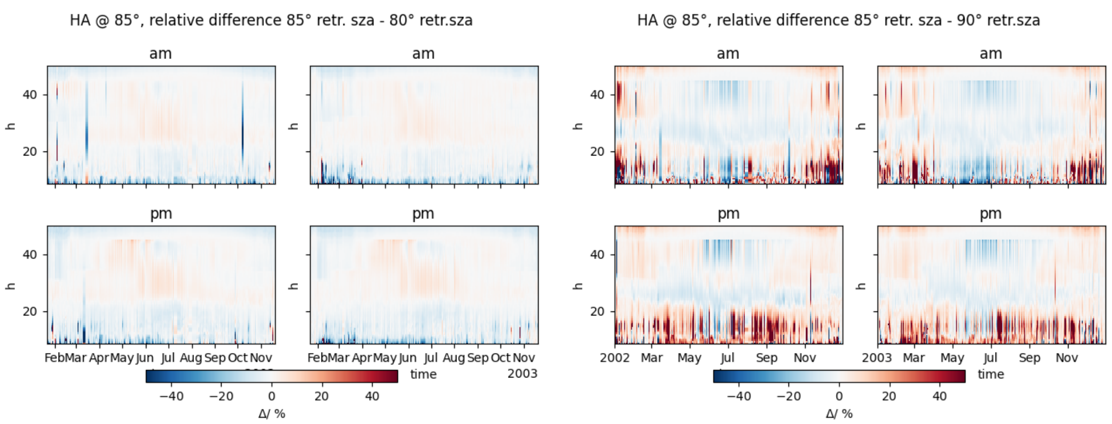

Figure 27: Relative difference as defined in Eq. 17 for A=85° and B=80° (left) and B=90° (right)

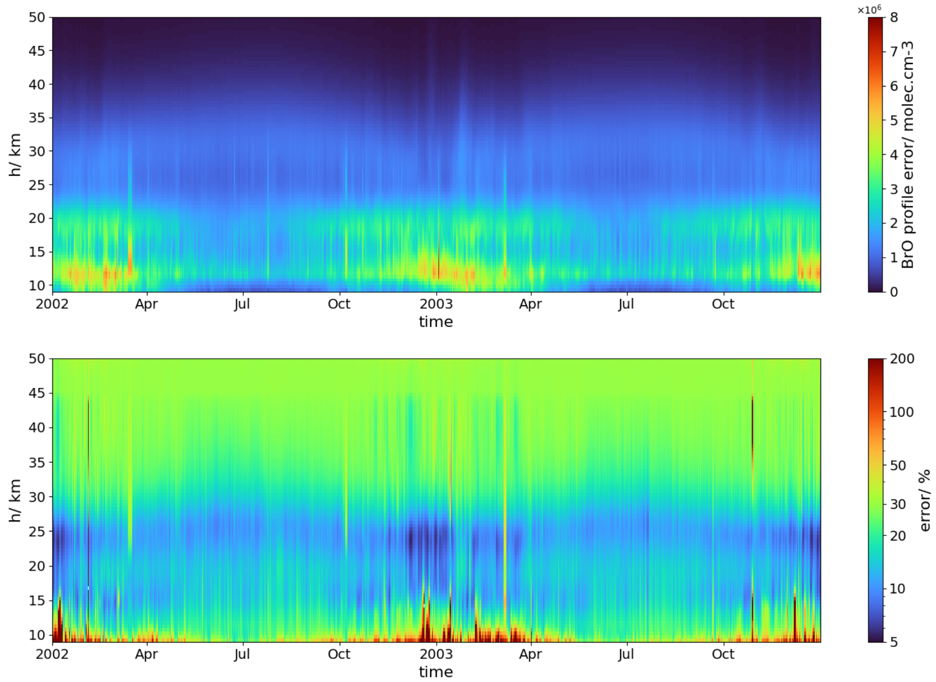

Figure 28: Combined smoothing and noise uncertainty for Harestua retrieval at sunrise 85° SZA, absolute error (top) and relative error (bottom)

6.4 Results at Kiruna

For Kiruna, (67.85° N, 20.30° E), the condition of reaching both 80° SZA and 90° SZA are not fulfilled during polar night or polar day, hence there are two distinct periods in which both ends of the retrieval range are reached, roughly from February to mid-May and from mid-July to November. We performed the retrieval for years 2002, 2022 and 2023 at 80°, 85° and 90° retrieval SZA. In Fig. 29 we show the retrieved stratospheric VCD at 90°, 80° and 85° SZA (top to bottom panel), each retrieved at all three SZAs, but only for years 2022 and 2023.

In order to better see possible systematic deviations, we also show the scatter plots (using all 3 years) in Fig. 29. As opposed to Harestua, the sunrise retrievals seem to show less variation and less systematic differences with retrieval SZA than the sunset retrievals, this is the opposite of what was seen at Harestua.

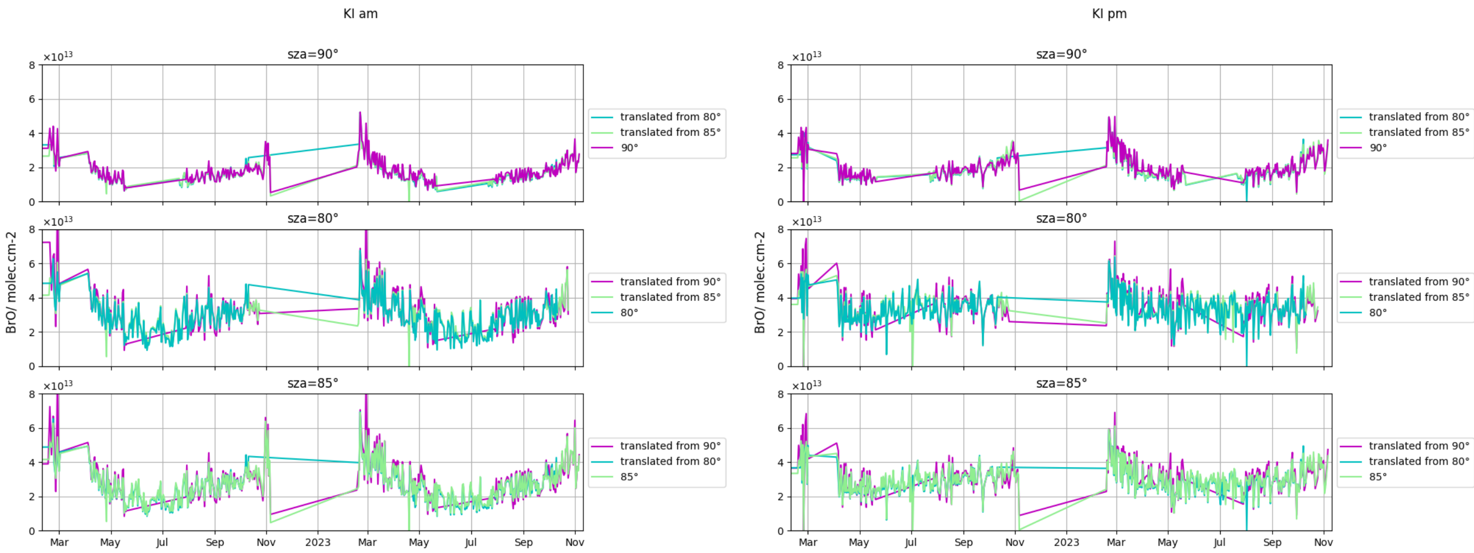

Figure 29: Time series of stratospheric VCD as in Fig. 18 but for Kiruna, left for sunrise retrievals, right for sunset retrievals.

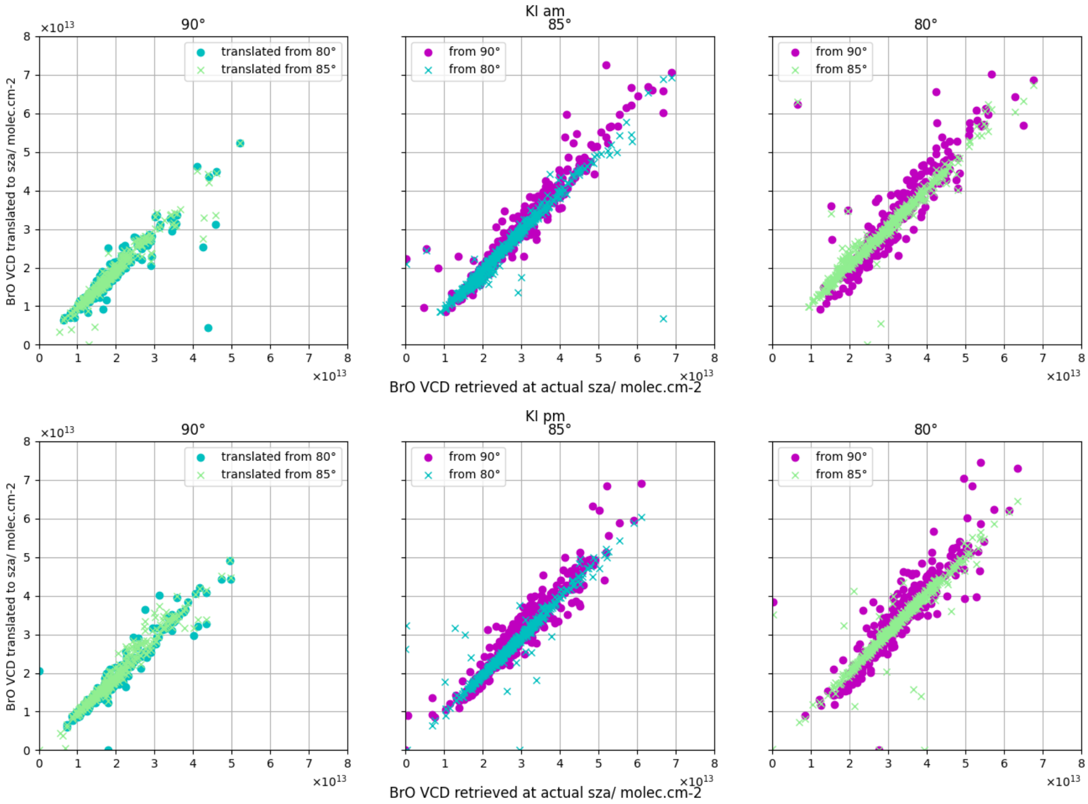

Figure 30: Scatter plots as in Fig. 25 but for Kiruna at 90°, 85° and 80° SZA, top panels for sunrise retrieval, lower panels for sunset retrievals.

7 Conclusion

We demonstrated that we can reproduce the results in NDACC GEOMS files for Harestua that were produced with an algorithm we try to reproduce if we choose the same retrieval settings for a limited number of days. Since we have not full access to the underlying *a priori* profiles at all SZA, we can only expect good agreement for days at which the underlying CTM in both retrievals show a similar SZA dependence of the profile.

We showed that at Harestua, there are systematic differences during late-spring and early-summer month (and also later summer months for sunrise retrievals) between stratospheric VCD in the NDACC GEOMS and data in Hendrick et al. (2007) that are derived from absolute SCD. The new retrievals agree better with the data from Hendrick et al. (2007).

We showed that often the retrieval SZA has a small effect on the retrieved stratospheric VCD but often a systematic effect on the retrieved profile. The difference in profile can be interpreted as an additional uncertainty, additional to the uncertainty from noise- and smoothing error.

For Kiruna we showed that the conclusions are similar as for Harestua.

Acknowledgments

Simon Chabrillat and Quentin Errera are the main developers of BASCOE. We are thankful for the permission of using BASCOE in the framework of FRM4DOAS and for the time and effort they put into helping us getting acquainted with the use. Further, we thank François Hendrick, who developed many of the prototype retrieval algorithms that this current work builds upon, for making his extensive code base available to us and for giving us a rough road map of the tasks. We thank Martyn Chipperfield for providing SLIMCAT data at Harestua which were used for additional initial testing ([c.f.] Deliverable:D8.2v.1) and Richard Querel for supplying spectra at Lauder.

A Results at Lauder

For Lauder (45.05° S, 169.68° E), as for Kiruna, we performed retrievals for years 2002, 2022 and 2023, using retrieval SZA 80°, 85° and 90°. Comparing, as for Kiruna, retrieved VCD at different SZA, we found large discrepancies. In Fig. 32 we show the same plot as shown for Kiruna in the upper panel (am) of Fig. 30.

We managed to identify the problem in the extraction of BASCOE data and plan to correct for this in the upcoming project. The station location of stations located in the southern hemisphere seems incorrect. This leads to wrong BrO profiles as function of SZA which leads to large (for 90°) and systematic (for 80° vs 85°) differences between retrievals performed at different SZA. While this is unfortunate, it is re-assuring that the proposed approach to use multiple SZA for the retrieval, revealed that there was a problem with the Lauder retrievals.

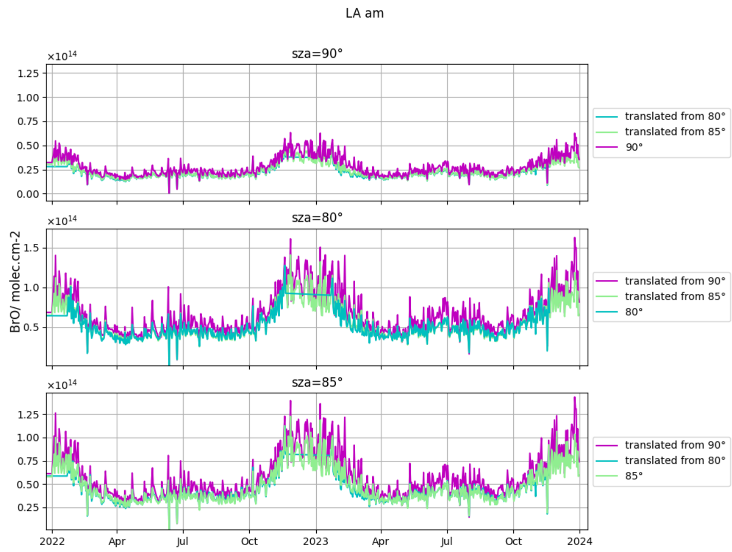

Figure 31: Time series of stratospheric VCD as in Fig. 18 at Lauder for sunrise retrievals.

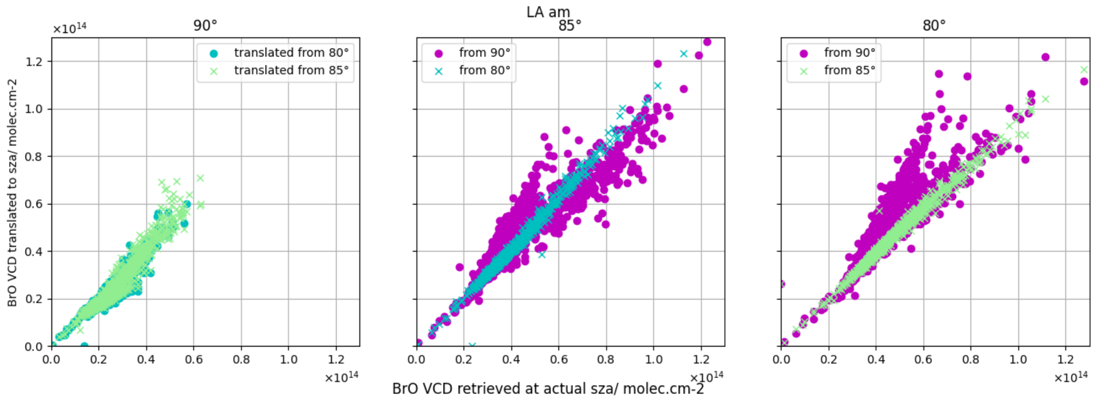

Figure 32: Scatter plots as in Fig. 25 but for Kiruna at 90°, 85° and 80° SZA, top panels for sunrise retrieval, lower panels for sunset retrievals.

References

Aliwell, S. R., T. Wagner, U. Platt, and K. Pfeilsticker (2002). “Analysis for BrO in zenith-sky spectra: an intercomparison”. In: *Journal of Geophysical Research* 107.D22, ACL 1–12. DOI: 10.1029/2001JD000329.

Bassford, M. R., K. Strong, C. A. McLinden, and C. T. McElroy (2005). “Ground-based measurements of ozone and NO_2 during MANTRA 1998 using a Zenith-sky spectrometer”. In: *Atmosphere-Ocean* 43.4, pp. 325–338. DOI: 10.3137/ao.430404.

Chabrillat, S., S. Rémy, Q. Errera, V. Huijnen, C. Bingen, J. Debosscher, F. Hendrick, S. Metzger, A. Mora, D. Minganti, M. Op de beek, L. Reisenfeld, J. E. Williams, H. Eskes, and J. Flemming (2025). “Modelling stratospheric composition for the Copernicus Atmosphere Monitoring Service: multi-species evaluation of IFS-COMPO Cy 49”. In: *Geoscientific Model Development* 18.22, pp. 8973–9014. DOI: 10.5194/gmd-18-8973-2025. URL: https://gmd.copernicus.org/articles/18/8973/2025/.

Chipperfield, M. P. (2006a). “New version of the TOMCAT/SLIMCAT off-line chemical transport model: Intercomparison of stratospheric tracer experiments”. In: *Q. J. R. Meteorol. Soc.* 132, pp. 1179–1203. DOI: 10.1256/qj.05.51.

Chipperfield, M. P. (2006b). “New version of the TOMCAT/SLIMCAT offline chemical transport model: intercomparison of stratospheric tracer experiments”. In: *Quarterly Journal of the Royal Meteorological Society* 132.617, pp. 1179–1203. DOI: 10.1256/qj.05.51.

Errera, Q., F. Daerden, S. Chabrillat, J. C. Lambert, W. A. Lahoz, S. Viscardy, S. Bonjean, and D. Fonteyn (2008). “4D-Var assimilation of MIPAS chemical observations: ozone and nitrogen dioxide analyses”. In: *Atmospheric Chemistry and Physics* 8, pp. 6169–6183. DOI: 10.5194/acp-8-6169-2008. URL: https://acp.copernicus.org/articles/8/6169/2008/.

Errera, Q. and D. Fonteyn (2001). “Four-dimensional variational chemical assimilation of CRISTA stratospheric measurements”. In: *Journal of Geophysical Research* 106, pp. 12253–12265. DOI: 10.1029/2000JD900828.

FRM4DOAS-2.0 (2005). *ATBD v1.* Deliverable D8.2v.1. FRM4DOAS-2.0.

FRM4DOAS-2.0:D1.2 (2022). *ATBD.* FRM4DOAS-2.0 D1.2. FRM4DOAS-2.0.

FRM4DOAS-2.0:D8.1 (2025). *Technical note on BrO Slant Column Fitting Optimisation.* FRM4DOAS-2.0 D8.1.

FRM4DOAS:D6 (2018). *MAXDOAS Algorithm ATBD.* FRM4DOAS D6. FRM4DOAS.

Geer, A. J., W. A. Lahoz, S. Bekki, N. Bormann, Q. Errera, H. J. Eskes, D. Fonteyn, D. R. Jackson, M. N. Juckes, S. Massart, V.-H. Peuch, S. Rharmili, and A. Segers (2006). “The ASSET intercomparison of ozone analyses: method and first results”. In: *Atmospheric Chemistry and Physics* 6, pp. 5445–5474. DOI: 10.5194/acp-6-5445-2006. URL: https://acp.copernicus.org/articles/6/5445/2006/.

Gomez-Martin, L., C. Prados-Roman, M. P. Chipperfield, M. Van Roozendael, O. Puentedura, M. Navarro-Comas, H. Ochoa, and M. Yela (2026). “UV/Vis Stratospheric Air Mass Factors considering photochemistry at two Antarctic stations”. In: *EGUsphere* 2026, pp. 1–31. DOI: 10.5194/egusphere-2026-17. URL: https://egusphere.copernicus.org/preprints/2026/egusphere-2026-17/.

Hendrick, F., B. Barret, M. Van Roozendael, H. Boesch, A. Butz, M. De Mazière, F. Goutail, C. Hermans, J.-C. Lambert, K. Pfeilsticker, and J.-P. Pommereau (2004). “Retrieval of nitrogen dioxide stratospheric profiles from ground-based zenith-sky UV-visible observations: Validation of the technique through correlative comparisons”. In: *Atmos. Chem. Phys.* 4, pp. 2091–2106. DOI: 10.5194/acp-4-2091-2004.

Hendrick, F., P. V. Johnston, K. Kreher, C. Hermans, M. De Mazière, and M. Van Roozendael (2008). “One decade trend analysis of stratospheric BrO over Harestua (60°N) and Lauder (45°S) reveals a decline”. In: *Geophys. Res. Lett.* 35, p. L14801. DOI: 10.1029/2008GL034154.

Hendrick, F., A. Rozanov, P. V. Johnston, H. Bovensmann, M. De Mazière, C. Fayt, C. Hermans, K. Kreher, W. Lotz, B.-M. Sinnhuber, N. Theys, A. Thomas, J. P. Burrows, and M. Van Roozendael (2009). “Multi-year comparison of stratospheric BrO vertical profiles retrieved from SCIAMACHY limb and ground-based UV-visible measurements”. In: *Atmospheric Measurement Techniques* 2.1, pp. 273–285. DOI: 10.5194/amt-2-273-2009. URL: https://amt.copernicus.org/articles/2/273/2009/.

Hendrick, F., M. Van Roozendael, M. P. Chipperfield, M. Dorf, F. Goutail, X. Yang, C. Fayt, C. Hermans, K. Pfeilsticker, J.-P. Pommereau, J. A. Pyle, N. Theys, and M. De Mazière (2007). “Retrieval of stratospheric and tropospheric BrO profiles and columns using ground-based zenith-sky DOAS observations at Harestua, 60deg; N”. In: *Atmospheric Chemistry and Physics* 7.18, pp. 4869–4885. DOI: 10.5194/acp-7-4869-2007. URL: https://acp.copernicus.org/articles/7/4869/2007/.

Hersbach, H., B. Bell, P. Berrisford, S. Hirahara, A. Horányi, J. Muñoz-Sabater, J. Nicolas, C. Peubey, R. Radu, D. Schepers, A. Simmons, C. Soci, S. Abdalla, X. Abellan, G. Balsamo, P. Bechtold, G. Biavati, J. Bidlot, M. Bonavita, G. D. Chiara, P. Dahlgren, D. Dee, M. Diamantakis, R. Dragani, J. Flemming, R. Forbes, M. Fuentes, A. Geer, L. Haimberger, S. Healy, R. J. Hogan, E. Hólm, M. Janisková, S. Keeley, P. Laloyaux, P. Lopez, C. Lupu, G. Radnoti, P. de Rosnay, I. Rozum, F. Vamborg, S. Villaume, and J.-N. Thépaut (2020). "The ERA5 global reanalysis". In: *Quarterly Journal of the Royal Meteorological Society* 146.730, pp. 1999–2049. DOI: 10.1002/qj.3803.

Horn, Roger A. and Charles R. Johnson (1990). *Matrix Analysis*. Cambridge, UK: Cambridge University Press, pp. xiii + 561. ISBN: 978-0-521-38632-6.

Huang, T., S. Walters, G. Brasseur, D. Hauglustaine, W. Wu, S. Chabrillat, X. X. Tie, C. Granier, A. K. Smith, S. Madronich, and G. Kockarts (1998). *Description of SOCRATES – a Chemical Dynamical Radiative Two-Dimensional Model*. Tech. rep. University Corporation for Atmospheric Research. DOI: 10.5065/D6K0726C. URL: https://doi.org/10.5065/D6K0726C.

Kylling, Arve and Bernhard Mayer (2003). *LibRadTran: A Package for UV and Visible Radiative Transfer Calculations in the Earth's Atmosphere*. URL: http://www.libradtran.org.

Mayer, B. and A. Kylling (2005). "Technical note: The libRadtran software package for radiative transfer calculations - description and examples of use". In: *Atmospheric Chemistry and Physics* 5.7, pp. 1855–1877. DOI: 10.5194/acp-5-1855-2005.

Mayer, B. (2009). "Radiative transfer in the cloudy atmosphere". In: *EPJ Web of Conferences* 1, pp. 75–99. DOI: 10.1140/epjconf/e2009-00912-1. URL: https://doi.org/10.1140/epjconf/e2009-00912-1.

Rodgers, C. D. (2000). *Inverse Methods for Atmospheric Sounding, Theory and Practice*. Singapore-New Jersey-London-Hong Kong: World Scientific Publishing.

Sander, S. P., R. R. Friedl, D. M. Golden, M. J. Kurylo, G. K. Moortgat, H. Keller-Rudek, J. R. Burkholder, R. E. Huie, V. L. Orkin, and P. H. Wine (2015). *Chemical Kinetics and Photochemical Data for Use in Atmospheric Studies, Evaluation No. 18*. JPL Publication 15-10. Jet Propulsion Laboratory, California Institute of Technology. URL: https://jpldataeval.jpl.nasa.gov/.

Sander, Stanley P., Jonathan P. D. Abbatt, John R. Barker, James B. Burkholder, Randolph R. Friedl, David M. Golden, Charles E. Kolb, Michael J. Kurylo, Geert K. Moortgat, and Paul H. Wine (2011). *Chemical Kinetics and Photochemical Data for Use in Atmospheric Studies, Evaluation No. 17*. Tech. rep. JPL Publication 10-6. Pasadena, California: Jet Propulsion Laboratory. URL: https://jpldataeval.jpl.nasa.gov/.

Skachko, S., R. Ménard, Q. Errera, Y. Christophe, and S. Chabrillat (2016). "EnKF and 4D-Var data assimilation with chemical transport model BASCOE (version 05.06)". In: *Geoscientific Model Development* 9.8, pp. 2893–2908. DOI: 10.5194/gmd-9-2893-2016. URL: https://gmd.copernicus.org/articles/9/2893/2016/.

Solomon, Susan (1999). "Stratospheric ozone depletion: A review of concepts and history". In: *Reviews of Geophysics* 37.3, pp. 275–316. DOI: 10.1029/1999RG900008.

Solomon, Susan, Arthur L. Schmeltekopf, and Ryan W. Sanders (1987). "On the Interpretation of Zenith Sky Absorption Measurements". In: *Journal of Geophysical Research: Atmospheres* 92.D7, pp. 8311–8319. DOI: 10.1029/JD092iD07p08311.

Stamnes, Knut, Si-Chee Tsay, Warren Wiscombe, and Kolf Jayaweera (1988). "Numerically stable algorithm for discrete-ordinate-method radiative transfer in multiple scattering and emitting layered media". In: *Applied Optics* 27.12, pp. 2502–2509. DOI: 10.1364/AO.27.002502.

Vervalcke, S., Q. Errera, S. Chabrillat, M. Op de beeck, T. Reddmann, G. Stiller, R. Eichinger, and E. Ma hieu (2025). "Atmospheric lifetime of sulfur hexafluoride (SF_6) and five other trace gases in the BASCOE model driven by three reanalyses". In: *EGUsphere* 2025, pp. 1–26. DOI: 10.5194/egusphere-2025-3597. URL: https://egusphere.copernicus.org/preprints/2025/egusphere-2025-3597/.

Vigouroux, C., M. De Mazire, Q. Errera, S. Chabrillat, E. Mahieu, P. Duchatelet, S. Wood, D. Smale, S. Mikuteit, T. Blumenstock, F. Hase, and N. Jones (2007). "Comparisons between ground-based FTIR and MIPAS N_2O and HNO_3 profiles before and after assimilation in BASCOE". In: *Atmospheric Chemistry and Physics* 7, pp. 377–396. DOI: 10.5194/acp-7-377-2007. URL: https://acp.copernicus.org/articles/7/377/2007/.

Wennberg, P. O., J. G. Anderson, F. Arnold, W. H. Brune, C. A. Cantrell, R. C. Cohen, N. M. Donahue, D. W. Fahey, F. Flocke, A. Fried, E. R. Keim, M. J. Kurylo, E. Mahieu, S. A. Montzka, C. E. Reeves, and R. J. Salawitch (1997). "Chemistry of the stratosphere: Halogen reactions and ozone depletion". In: *Science* 276, pp. 1036–1039. DOI: 10.1126/science.276.5315.1036.